64-9

TECHNICAL INFORMATION SERIES

R63SD84

PYROLYTIC GRAPHITE-A STATUS REPORT

A.M. GARBER
E.J. NOLAN
S.M. SCALA

SPACE SCIENCES LABORATORY
GENERAL ELECTRIC
MISSILE AND SPACE DIVISION

RE-ENTRY SYSTEMS DEPARTMENT
SYSTEMS AND TECHNOLOGIES SECTION
AND
SPACE SCIENCES LABORATORY
AEROPHYSICS SECTION

PYROLYTIC GRAPHITE - A STATUS REPORT*

By

A. M. Garber
E. J. Nolan
S. M. Scala

*Based on work supported in part by USAF Ballistic Systems Division, Contract No. AF 04(694)-222

R63SD84
October, 1963

MISSILE AND SPACE DIVISION

GENERAL ELECTRIC

CONTENTS

ABSTRACT

It is the purpose of this paper to review the recent history of the development of pyrolytic graphite and its thermal, aerothermochemical, and structural properties with regard to its application to hypersonic vehicles.

Pyrolytic graphite is not really new since its discovery dates back to Thomas Edison, however, this class of refractory materials has been "rediscovered" recently because it possesses certain desirable properties at extremely high operating temperatures, including a high strength to weight ratio, low oxidation rate, and a low transverse coefficient of thermal conductivity.

Consequently, a thorough investigation of the properties of pyrolytic graphite is being carried out. In addition, theoretical models are being developed so that its aerothermochemical and aerothermostructural behavior can be predicted with confidence for arbitrary hypersonic missions. In this paper, the currently available property data, and analytical and numerical techniques are presented and discussed critically, and areas for future research and development are delineated.

PYROLYTIC GRAPHITE - A STATUS REPORT

A. M. Garber, E. J. Nolan and S. M. Scala
General Electric Company
Missile and Space Division
Philadelphia 1, Pennsylvania

INTRODUCTION

One of the newer refractory materials which has received a certain amount of emphasis for hypersonic applications during the past few years is pyrolytic graphite.

Surprisingly, pyrolytic graphite is not really new since its discovery dates back to Thomas Edison (1). One of the interesting features of pyrolytic graphite which makes it attractive for hypersonic vehicles is the high degree of anisotropy of this material in both its physical and mechanical properties and its low rate of oxidation (ablation).

Indeed, several years ago, its use was considered in one of the active missile programs, but because of certain logistics problems that arose, it was not chosen for flight hardware. Intensive materials efforts during this particular program gave rise to the first full scale manufacturing effort based on the vapor deposition of pyrolytic graphite. Prior to this time, only small pieces had been made on a laboratory scale, by Edison in his incandescent lamp work, and more recently by several other investigators.

Pyrolytic graphite may be produced by thermally decomposing a hydrocarbon gas, such as methane, and depositing the carbon on a hot surface, under carefully controlled conditions. One method now in use consists of heating the hydrocarbon gas to temperatures ranging up to 5000°R, in a vacuum furnace, see Fig. (1). During the decomposition of the gas, gaseous carbon deposits on the surface of a prepared mandrel which is usually commercial graphite. The carbon atoms formed during the cracking process, then condense on the substrate in an orderly fashion, layer upon layer, producing an ordered structure which has a higher strength to weight ratio than commercial graphite, see Fig. (2), and hence is potentially more attractive for aerospace applications. Some typical specimens of pyrolytic graphite are shown in Fig. (3).

The separate hexagonal layer planes of pyrolytic graphite are all parallel to the

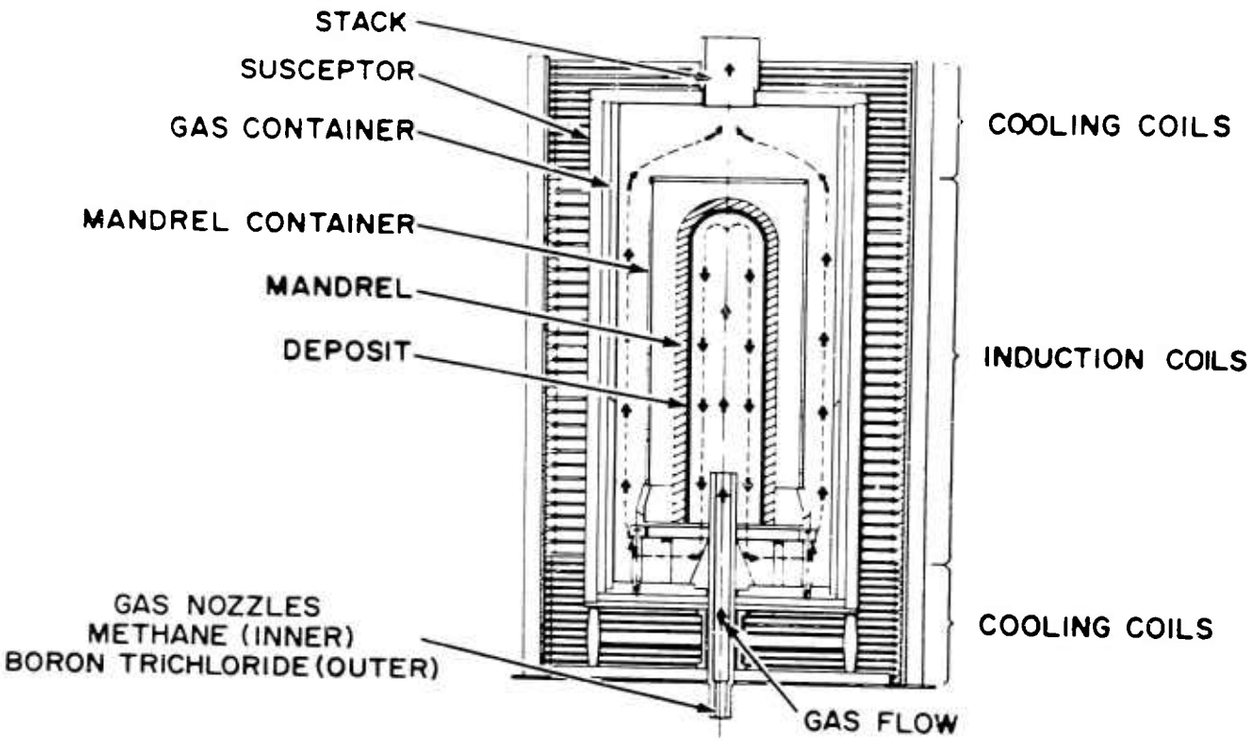

Fig. 1. A Typical Pyrolytic Graphite Furnace Assembly

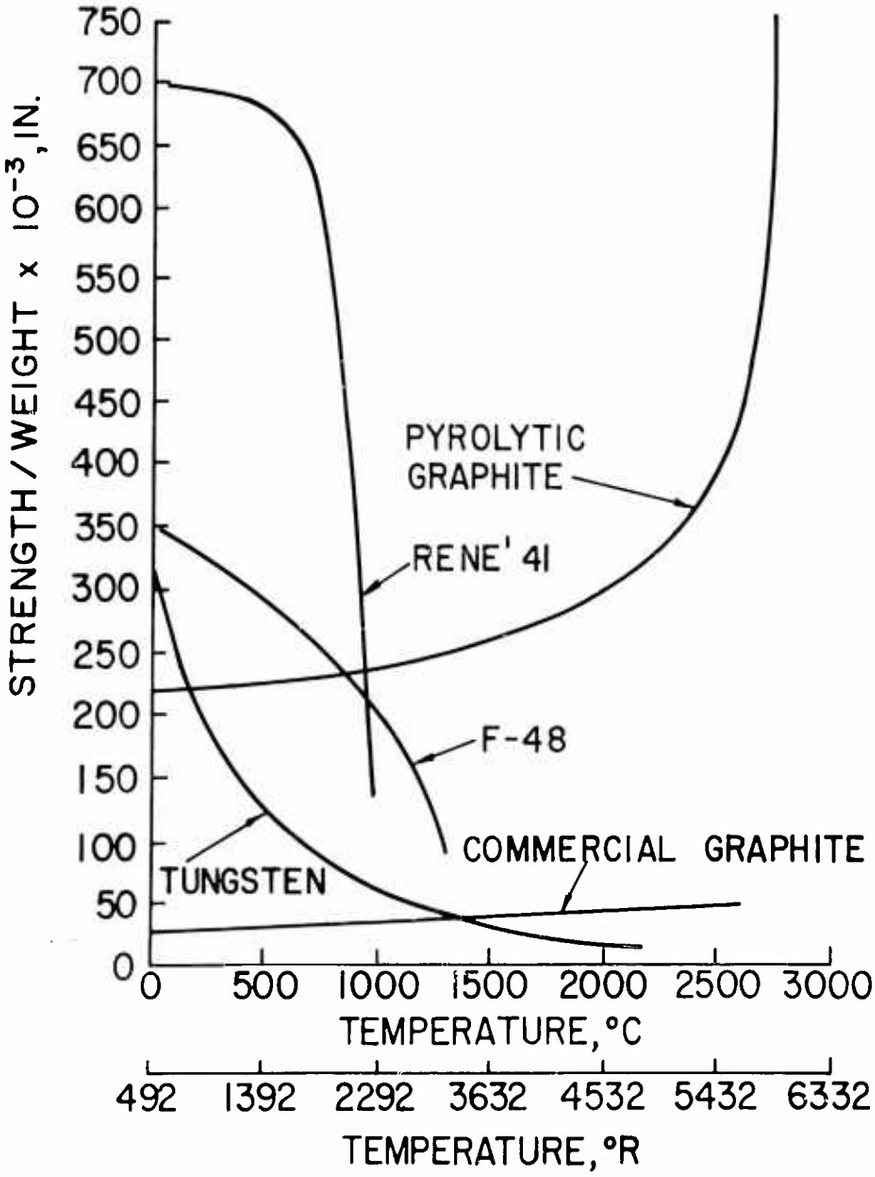

Fig. 2. Strength to Weight Ratio vs. Temperature

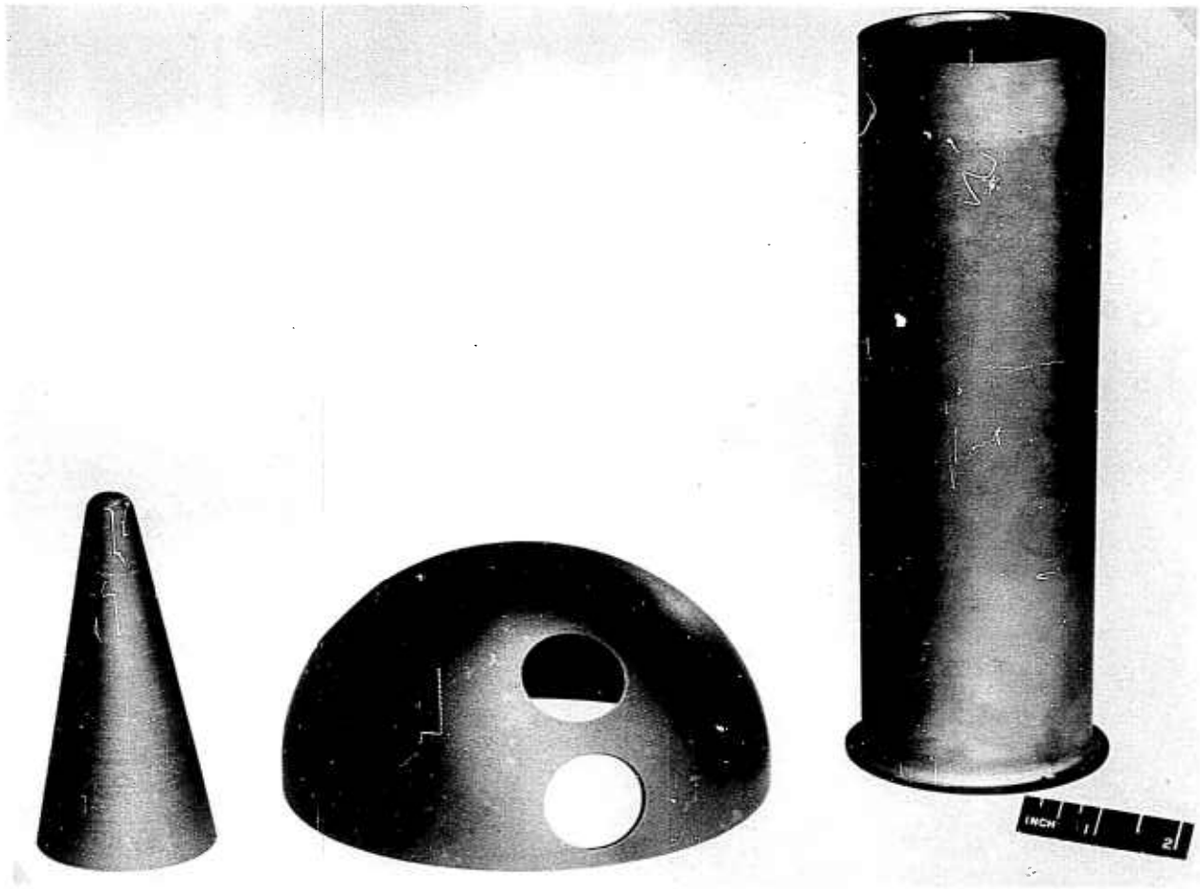

Fig. 3. Three Representative Pyrolytic Graphite Specimens

basal (deposition) plane (a-b plane), but do not have the regular appearance of a honeycomb with respect to each other. Microscopic examination shows that pyrolytic graphite is a highly oriented crystalline structure resembling densely packed stalagmites, see Fig. (4).

In the case of commercial graphite, the layer planes have a random orientation for the different crystallites; there are approximately two crystals oriented normal to the surface ("c" axis), for every crystal oriented parallel to the surface (a-b plane). In contrast, the crystals of pyrolytic graphite are highly oriented, so that the number oriented in the "c" direction is two or three orders of magnitude for every one in the a-b orientation. The high degree of anisotropy in the structure of pyrolytic graphite results in a high degree of anisotropy in all of its thermal properties, (except the specific heat).

During the early manufacturing phases of the full scale hardware of pyrolytic graphite in the missile program mentioned above, certain problems arose that were not evident during the laboratory effort, resulting in what appeared to be random cracking, delamination and spallation of the freestanding piece as manufactured. It was observed further that hardware which appeared to be of sound quality would often fail upon exposure to heating in arcs and rocket engine exhausts. The nature of these failures was similar to those occurring in the freestanding manufactured piece. An exhaustive investigation into the causes of these failures was undertaken by the manufacturers involved in this missile program and within six months, a number of interesting results were obtained.

It was found for example, that nodule formation, which was a source of stress concentration, and therefore potential failure, could be minimized by improving certain process parameters and the housekeeping procedures around the process equipment. The question as to why delamination and cracking of the manufactured pyrolytic graphite can occur, involves a thorough understanding of the behavior of brittle anisotropic materials, the technique of deposition and the subsequent stresses which arise during the deposition process and the cooling down period. This stress interplay and its importance was recognized, (2) during this investigation period. Techniques for computing the magnitude of these stresses in an anisotropic material could not be developed in such a short period of time. However, enough of the overall problem, including proper design of the specimen under test, was sufficiently well understood to permit some thirteen straight successful experiments to be performed in a 15" diameter Vanguard rocket engine exhaust. It is noteworthy that full scale experimental hardware was used during these tests.

During and subsequent to the aforementioned pyrolytic graphite development effort, the investigation of analytical techniques for the prediction of mass transfer, heat transfer and the structural response of pyrolytic graphite during atmospheric flight at hypersonic speeds was initiated at the General Electric Company. Several reports of different phases of this effort have already appeared in the literature, see

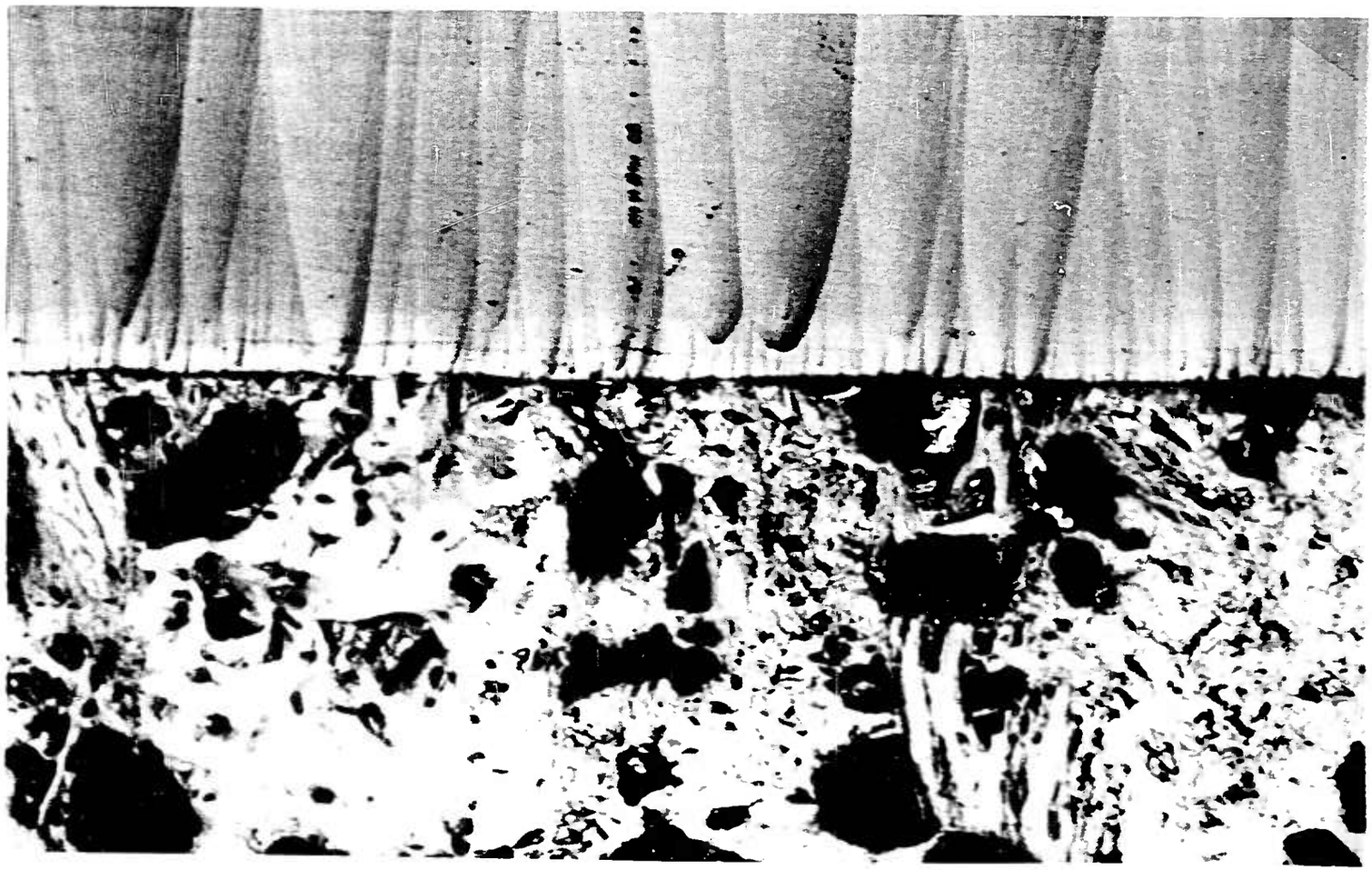

Fig. 4. Photomicrograph of Pyrolytic Graphite Deposited on Commercial Graphite

(3), (4), (5) and (6). It has been found, for example, that by correct mandrel design and control of certain variables during deposition, freestanding pieces can be prepared that would experience thermal stresses during flight which are lower in magnitude than those obtained during manufacture and the subsequent cool-down process. It has been found also that a change in the degree of anisotropy can likewise change the thermal stress distribution produced during flight, depending on the level and direction of the anisotropy.

These results will be reviewed in more detail in a later section.

CHEMICAL KINETICS

In considering the chemical aspects of the performance of pyrolytic graphite, one quickly notes a certain paradoxical situation. That is, although the chemical reactions between carbon and oxygen have been studied for well over one hundred years, nevertheless an incomplete understanding of the mechanism of mass loss exists even for ordinary graphite. Although it is known for a certainty that in the low surface temperature regime where the oxidation process is rate controlled, the volatile reaction products CO_2 and CO are produced, it has not yet been established as to what the actual sequence of steps is, nor has the slowest, and hence rate determining, step been determined. Consequently, it is both useful and necessary to introduce the following empirical Arrhenius representation for the oxidation rate in the reaction rate controlled oxidation regime

$$\dot{m}_R = k \left(P_{O_2} \right)_w^n \tag{1}$$

where k is the specific reaction rate, $\left(P_{O_2} \right)_w$ is the partial pressure of molecular oxygen near the surface, and n is the order of the reaction.

An examination of the available experimental data (7), (8), indicates that although n is bounded, there is some disagreement as to the precise magnitude of n. Further, upon writing the specific reactivity in the form (9),

$$k = k_o e^{-E/RT_w} \tag{2}$$

it is seen that in order to specify the chemical kinetic behavior of pyrolytic graphite, one requires a knowledge of E, the activation energy and k_o, the effective collision frequency.

Upon making use of the data appearing in Ref. (9), one finds that for graphitic materials, the following bounds on the chemical kinetic properties apply: (see Fig. (5))

$$0 < n < 1.0 \tag{3}$$

$$8 < E < 60 \text{ Kcal/mole} \tag{4}$$

$$1 < k_o < 10^9 \text{ lb./ft.}^2 \text{ sec.} \tag{5}$$

This extremely wide range in chemical kinetic data for graphite may be attributed to the fact that these properties depend critically on how the material was manufactured. Thus, since there are at least as many different grades of graphite as there are manufacturers (with different quality control procedures), it is unlikely that any two investigators have tested the same material.

At the moment, the only useful data on the oxidation rate of pyrolytic graphite is due to Horton (10). However, as has been pointed out by Nolan and Scala (4), there is sufficient scatter in his data to question his optimistic (extremely low mass loss) interpretation of the data. Consequently, at this moment we can quote two sets (4), (optimistic and conservative) of chemical kinetic data, based on one set (10), of experimental measurements for the oxidation of pyrolytic graphite.

$$\begin{cases} E = 32.8 \text{ Kcal/mole} \\ k_o = 3.07 \text{ lb./ft.}^2 \text{ sec.} \end{cases} \tag{6a}$$

$$\begin{cases} E = 47.5 \text{ Kcal/mole} \\ k_o = 1.28 \times 10^4 \text{ lb./ft.}^2 \text{ sec.} \end{cases} \tag{6b}$$

It is noted that the value of n to be used with the data of Eq. (6a) or (6b) is n = 1/2. For the case of n = 1/2, and for low surface temperatures, in the rate controlled oxidation regime, since the pressure gradient at the surface is negligible, one can write for the partial pressure of oxygen at the surface,

$$\left(P_{O_2}\right)_w \approx \left(X_{O_2}\right)_w P_e \tag{7}$$

and hence, there follows immediately:

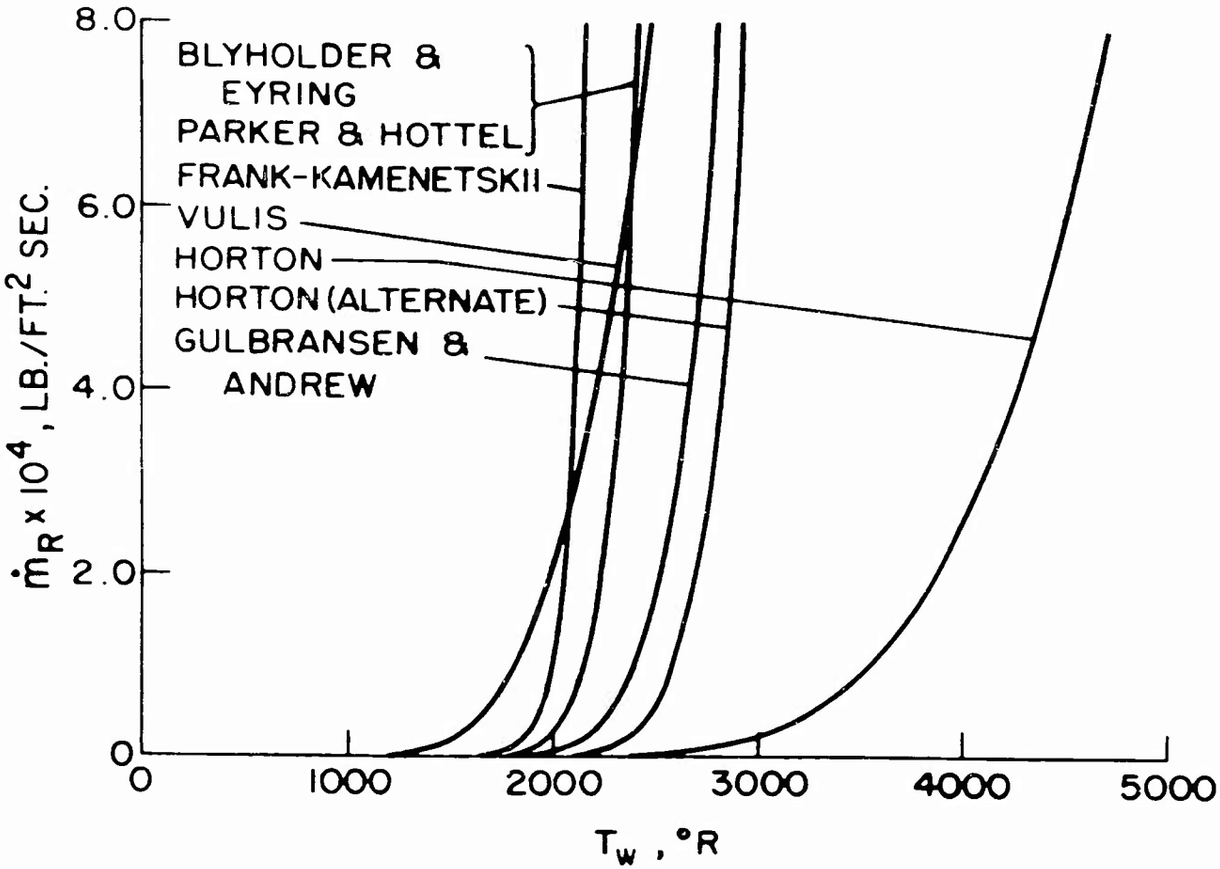

Fig. 5. Rate Controlled Oxidation Data, (P = 0.1 atm.)

$$\frac{\dot{m}_R}{\sqrt{P_e}} = k_o \left(X_{O_2} \right)_w^{1/2} e^{-E/RT_w} \tag{8}$$

where, in first approximation,

$$\left(X_{O_2} \right)_w = 0.21. \tag{9}$$

It is expected that Eq. (8) will apply even when the free stream air is dissociated provided that the gas phase reaction rates are sufficiently fast so that the atomic oxygen has recombined to the molecular state before colliding with the surface. If the gas phase reaction rates are either "frozen", or so slow that oxygen atom recombination is not complete in the gas phase, then the rate constants given in Eq. (6) are not applicable, since atomic and molecular oxygen react with carbon at different rates (11).

THERMAL AND STRUCTURAL PROPERTIES

Even though pyrolytic graphite is not a new material, a significant attempt to measure its properties has only been made recently, (12) through (22), and a review of information available since 1959 on certain properties of pyrolytic graphite has recently been made, (23). For data to be reliable, and to insure proper deductions from theoretical calculations, it is essential that the experimental data be obtained for pyrolytic graphite that has been manufactured under controlled conditions. In particular, all of the properties should be determined for specimens from the same manufactured batch.

However, in practice, it appears that the acquisition of properties of a particular identifiable pyrolytic graphitic material is difficult. Because of manufacturing and physical variables that occur during deposition, such as grain size, pressure changes and changes in flow rate, one may expect that one type of pyrolytic graphite manufactured in one facility need not necessarily be the same as that from another. As a consequence of these process variations, substantial variations in the property values have been reported in the literature. Unfortunately, in some instances, the data reported in the literature does not identify the material from which the data was obtained.

In reviewing the literature, it has been found also that the details of the experimental procedure have not been given adequately. For example, the preparation of samples may introduce delaminations, which can affect the strength.

It should be noted that it is difficult to measure stresses and strains in pyrolytic graphite because of its brittle nature at relatively low temperatures. In making these measurements small bending stresses can appreciably alter measured fracture stresses.

When making measurements at elevated temperatures difficulties are introduced because of anisotropic expansion, and further difficulties arise because of the lack of a good technique in accurately measuring high surface temperatures in a range from 4500°R to 5500°R. It should also be mentioned that certain qualifications are necessary prior to the application of data obtained on flat-wall machined specimens to curved shapes such as might be found on hypersonic vehicles.

It has been observed (23) that machining can introduce surface defects which might induce fracture failures far sooner than would be the case with smooth undamaged surfaces. Of course, this does not apply to such values as the elastic modulus, thermal conductivity and coefficient of expansion. When measuring the high temperature properties (above 3600 R), one should also take into account the probability that pyrolytic graphite becomes translucent and that phonon transport plays a significant role in defining the apparent thermal conductivity.

By far, the largest amount of data available has been published as a Lockheed Missiles and Space Company report (20). Unfortunately, however, the data presented is not readily identifiable with a well-characterized material, and hence its usefulness is severely limited. Insofar as data reported in the literature are concerned, the reports issued by the Raytheon Company (21) and Aerojet General (22) are quite complete. Their evaluation of the experimental difficulties involved ir making pyrolytic graphite measurements and the necessity of correlating measured data to a well-defined material show an appreciation for the experimental techniques and manufacturing difficulties associated with anisotropic materials. However, this is not to imply that the materials used in their experiments were always satisfactory. Indeed, the reports (22) state that specimens were received, and presumably used, in which defects such as chips, partial delaminations and large nodules were visible.

The only data reported which considered the effect of structure on properties were found in a summary report issued by Raytheon, (21). A microstructural classification technique was used to identify the material. Both mechanical and thermal properties were obtained for several different types of microstructures which varied from surface nucleated to highly regenerative material. The majority of the data is based on highly regenerative material, but enough work was performed on a surface nucleated structure to allow comparison. These two structures differ considerably from each other and hence may be taken as approximate bounds when considering the property variations of pyrolytic graphite.

The coefficient of thermal expansion for surface nucleated and the highly regenerative continuously nucleated materials in both the "a" and "c" directions is shown in Figs. (6) and (7). The regenerative material which has more contributions from the "c" direction, shows a significantly higher coefficient of expansion. On the other hand, the "c" direction coefficient of expansion (Fig. 7) seems to be independent of microstructure.

The thermal conductivity coefficient for both the "a" and "c" directions is shown in Figs. (8) and (9). The regenerative material has a slightly higher conductivity, which

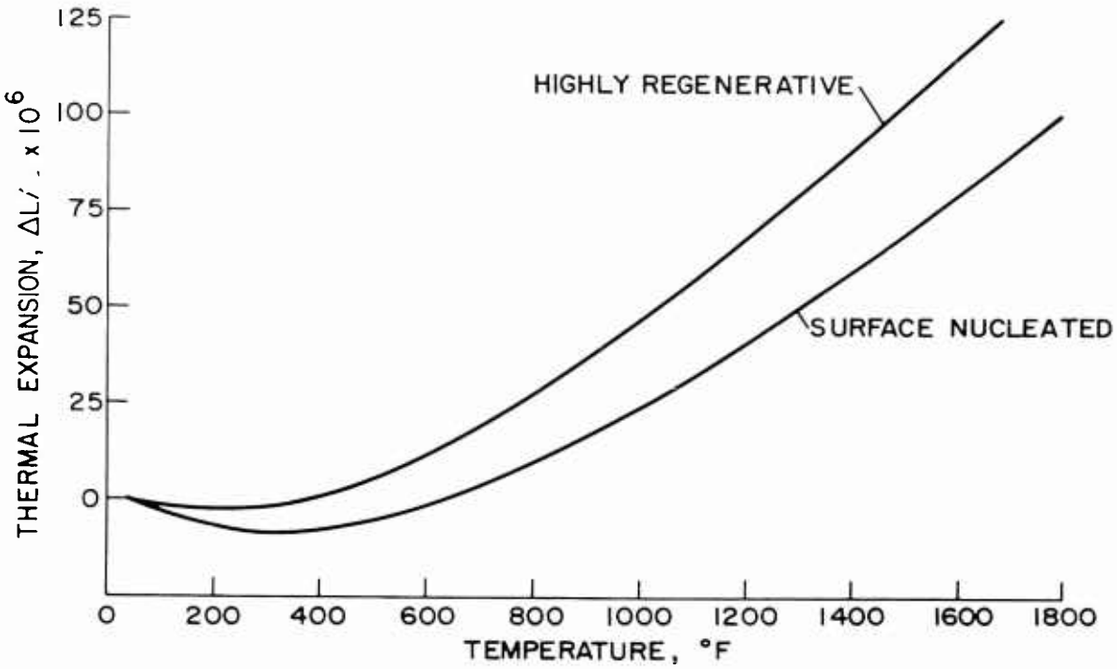

Fig. 6. Coefficient of Thermal Expansion of Pyrolytic Graphite in "A" Direction for Two Microstructures

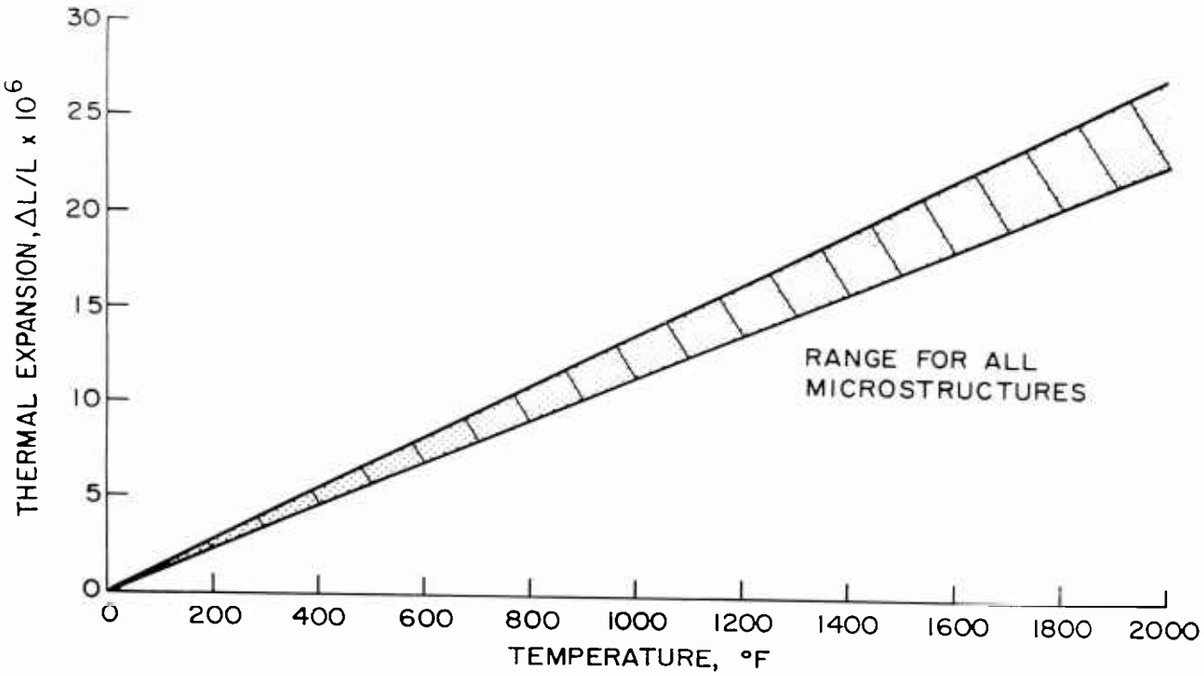

Fig. 7. Coefficient of Thermal Expansion of Pyrolytic Graphite in "C" Direction for Various Microstructures

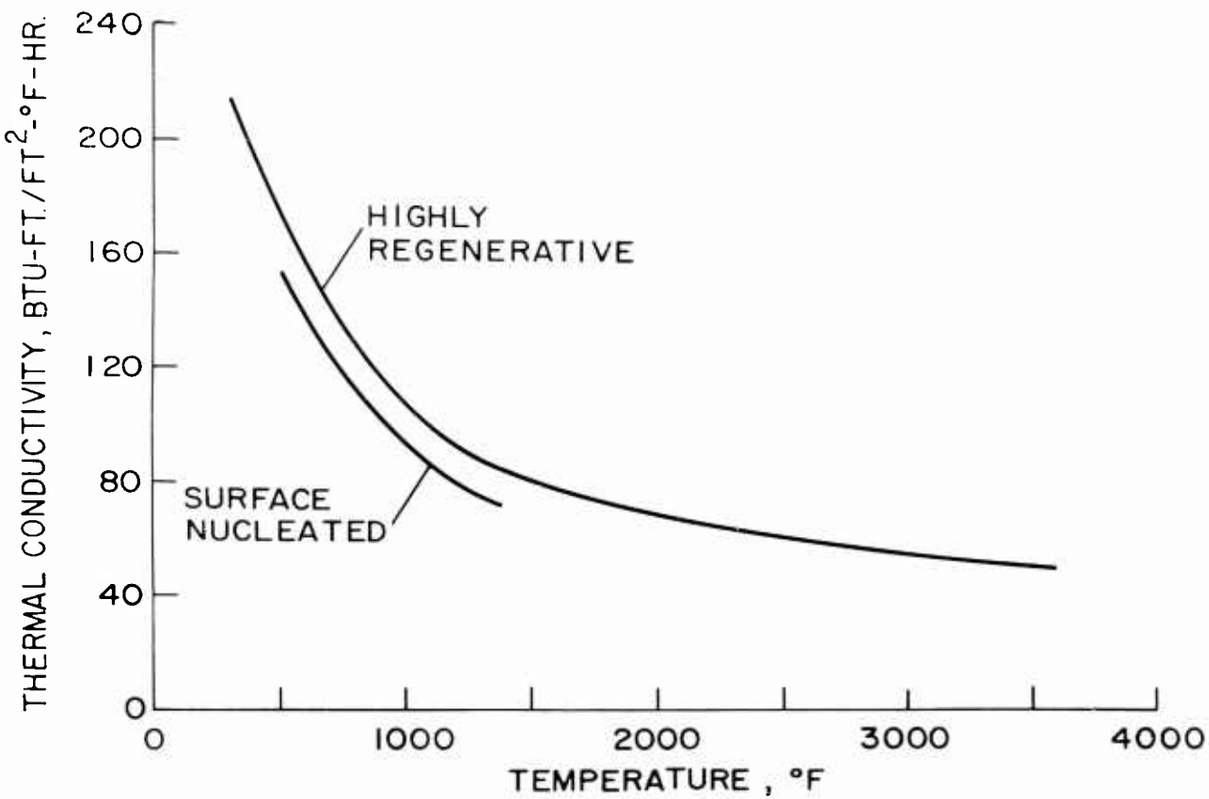

Fig. 8. Thermal Conductivity of Pyrolytic Graphite in "A" Direction for Two Microstructures

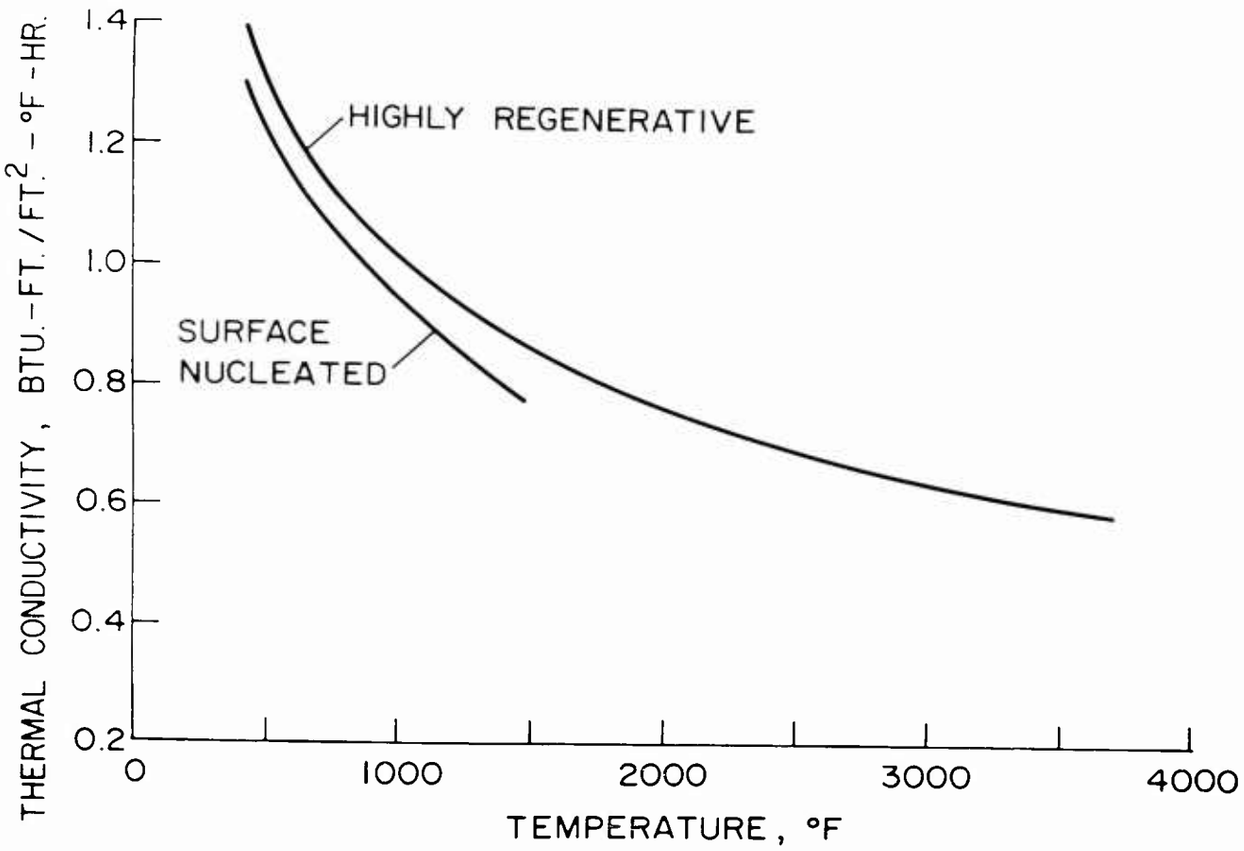

Fig. 9. Thermal Conductivity of Pyrolytic Graphite in "C" Direction for Two Microstructures

may or may not be extrapolated to higher temperatures because of the increasing role of phonon transport. The difference, however, is not large. It should be pointed out that heat treatment at 2900°C for two hours can increase the "a" direction conductivity by about a factor of three, (21).

Dynamic modulus data (21) are shown in Fig. (9). The data are interesting from several respects. An anomalous increase in modulus in a range of temperatures from 250° to 700°F is shown together with the expected linear decrease in modulus with an increase in temperature above 700°F. In the absence of relaxation, this linear decrease is to be expected for normal polycrystalline materials. Fig. (10) shows that the modulus decreases linearly from 1750° to 2250°F; but between 1000° and 1750°F shows a departure from linearity. This type of behavior has often been noted for polycrystalline materials and is attributed to grain boundary plastic flow. In pyrolytic graphite, the behavior may be due to microscopic viscous flow between conical crystallite boundaries. If this is indeed the case, some relaxation of residual stresses may be expected in this temperature range.

The dynamic modulus of the surface nucleated material is slightly higher than the regenerative material throughout the temperature range 75° to 2250°F. The static room temperature moduli, also shown on Fig. (10) are somewhat higher but bear the same relation to one another, as do the dynamic moduli.

The difference in magnitude between static and dynamic values was not discussed in Ref. (21), but may well be due to using the resonant frequency obtained experimentally and computing the modulus on the basis of isotropic elastic theory. In general, static and dynamic moduli for isotropic polycrystalline metals, in the absence of relaxation, are equal (24).

It is not realistic to use the temperature dependence of the dynamic modulus and apply it to the static values because of the (presumed) conical boundary flow between 750° and 1750°F. This behavior, whatever the cause, leads to a 45% drop in the dynamic modulus between 75°F and 2250°F. On the other hand, recent data obtained by GE show that the static modulus of a highly regenerative material is essentially constant from 75°F to 3000°F changing only from 3.5 to 3.4 x 10^6psi. The cause of the temperature variation of the dynamic modulus, and associated variation of the internal friction, is not fully understood but should be studied further.

The values reported in Ref. (21) for the static elastic modulus of the regenerative structure are:

Static Modulus of Regenerative Material	Tension, psi.	Compression, psi.
"a" Direction	4.0-4.4 x 10^6	4.1 x 10^6
"c" Direction	1.6 x 10^6	1.6 x 10^6

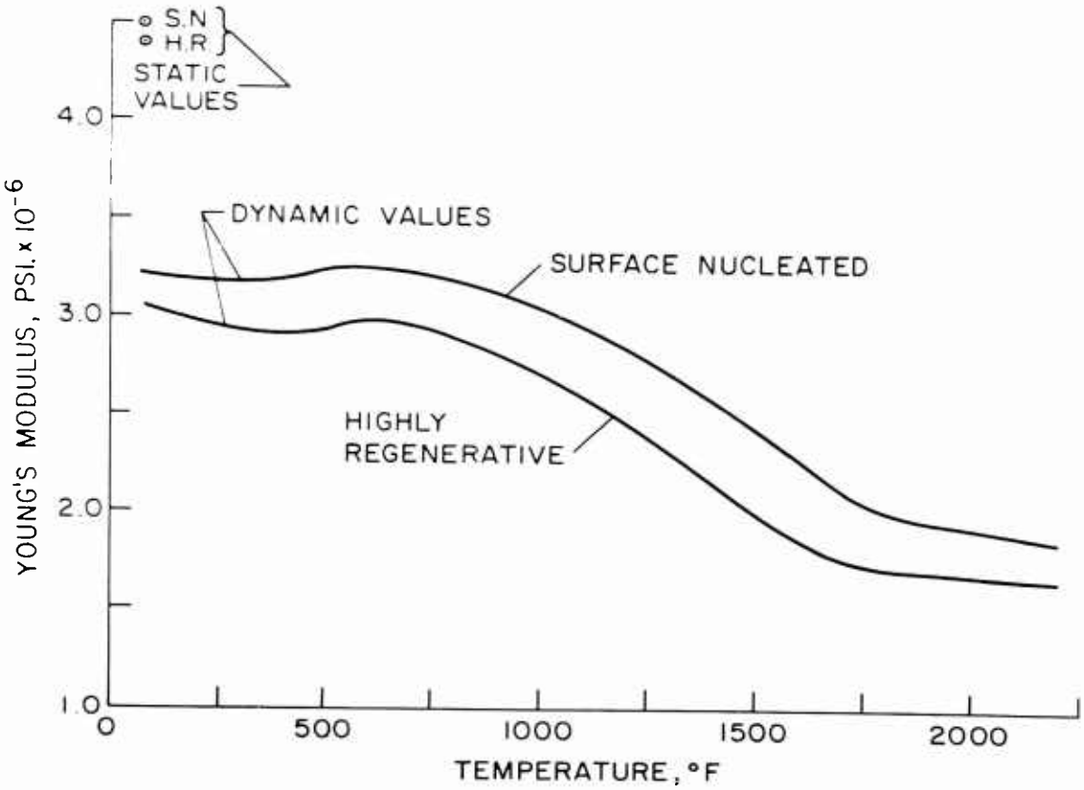

Fig. 10. Static and Dynamic Modulus of Pyrolytic Graphite in "A" Direction for Two Microstructures

These values are slightly higher than the foregoing data, but indicate that the tensile and compressive moduli are similar. The difference between the data may well be due to different manufacturing techniques.

Kotlensky and co-workers at JPL have published several reports dealing with PG over the past several years (25) through (28). The data include only tensile tests, and are shown in Table (1). The data are plotted in Fig. (11), together with 50% confidence limits (20). The Jet Propulsion Laboratory data seem to conform to the 50% curve. These data also show mechanical properties of pyrolytic boron nitride. It will be noted that the low temperature strength appears to be lower than that of pyrolytic graphite.

Work has also been performed recently (29) at General Electric - MSD. Data obtained (but not presented here), include both continuously nucleated and surface nucleated material. A report is currently in preparation and stress-strain curves will be available. Other data obtained as part of the aforementioned work are the coefficient of thermal expansion, shear strength in the a-b plane, and three and four point loaded bend tests, all measured at temperatures up to 5000°F. The new data for pyrolytic graphite shows appreciably higher strength than both the Lockheed and JPL data. As a consequence of this study, these investigators are lead to conclude that "pyrolytic graphite as it is currently made and tested, is a considerably stronger and more reliable material than was the case earlier in its development". This may be attributed to both improved process control and a better understanding of the effects of surface damage on the properties of pyrolytic graphite. Care in selection of representative material, inspection of specimens before testing and of fracture surfaces after testing must become part of the routine test procedure to insure that quoted results correspond to the mode of failure actually produced and that they do not reflect the effects of notches, nodules, delaminations or machine damage.

It is further believed by these investigators that the maximum inherent strength of pyrolytic graphite has yet to be achieved in test specimens. Studies of the basic processes by which fracture is initiated and propagated have lead to the conclusion that cutting and machining of test specimens leads inevitably to the presence of stress concentration on all surfaces. "The strength as measured is thus not indicative of the inherent strength of pyrolytic graphite, but rather of a specimen which has already been damaged". Improved machining and finishing techniques are currently under study as well as methods of restoring surfaces to a relatively undamaged status. However, there is a need for developing a general design and fabrication technology for pyrolytic graphite as well as for the newer vapor-deposited refractory anisotropic materials which are currently undergoing exploratory evaluation. The demand for some of their unique properties is pressing enough to carry their study beyond the preparative stage to a level where they are practical materials of construction.

A recent review article (23) has summarized the difference in behavior between pyrolytic graphite (PG), boron pyrolytic graphite (BPG), and boron nitride (BN), with respect to thermal conductivity. These data are shown in Fig. (12). In addition, the

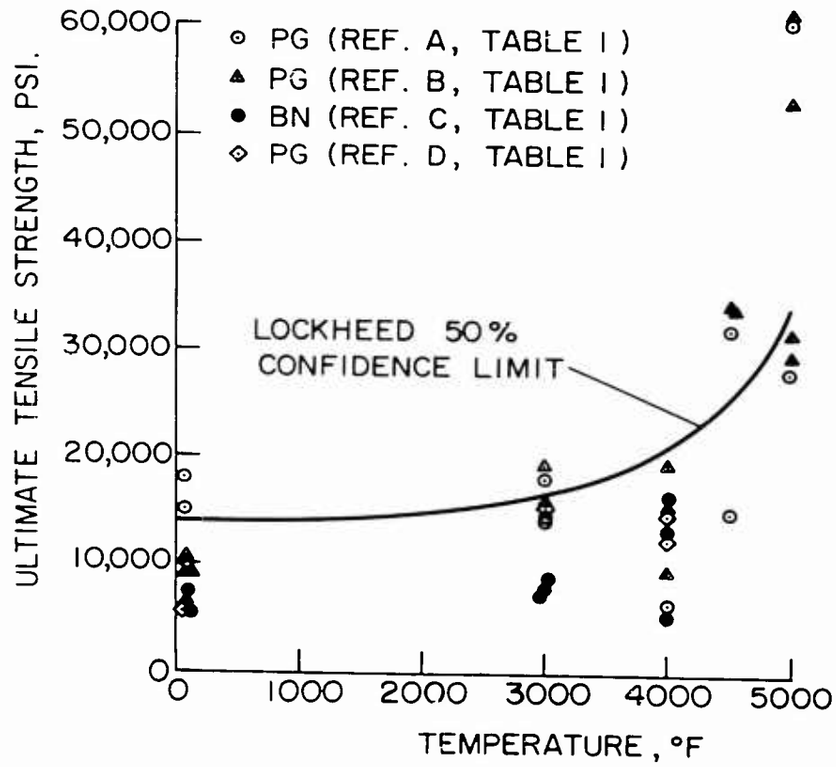

Fig. 11. Ultimate Tensile Strength of Pyrolytic Materials

Table 1. Tensile Tests on Pyrolytic Graphite and Boron Pyrolytic Graphite in a-b Direction

Test Temp. °F	PG-Raytheon[a] σ, psi.	% Elong.	PG-Raytheon[b] σ, psi.	% Elong.	BN-HTM[c] σ, psi.	% Elong.	PG-GE[d] σ, psi.	% Elong.
75	15,000	-	9050	0.1	5370	1.6	10,000	-
	18,000	-	10,670	0.1	5260	2.0		
			9260	0.1	6980	1.1		
			6510	0.2				
3000	18,000	-			7800	1.0	15,500	-
	14,000	-	19,470	4.4	7360	0.5		
	14,500	-	15,930	4.0	8760	0.5		
4000	6500	-	9300	2.8	5620	0.6	12,600	-
			15,670	1.8	13,200	2.5	14,900	-
			19,420	2.8	16,400	3.6		
4500	15,000	-	34,100	7.6				
	32,000	-	34,110	5.5				
4990	60,000	-	29,680	24.0				
	28,000	-	60,860	59.0				
			31,600	18.0				
			50,310	26.0				

(a) Deposited at 2100°C; Sp. Grav. = 2.20; Lockheed MSC Report FL 11379-A, June 1961.
(b) Deposited at 2100°C; Sp. Grav. = 2.19 - 2.21; Lockheed MSC Report FL 11379, February 1961.
(c) Deposited at 1900°C on graphite; Gas: boron chloride plus ammonia; Sp. Grav. = 2.1; Lockheed MSC Report FL 10407-B, April 1961.
(d) Deposited at 2100°C; Sp. Grav. = 2.19; Lockheed MSC Report FL 11465-C, August 1961.

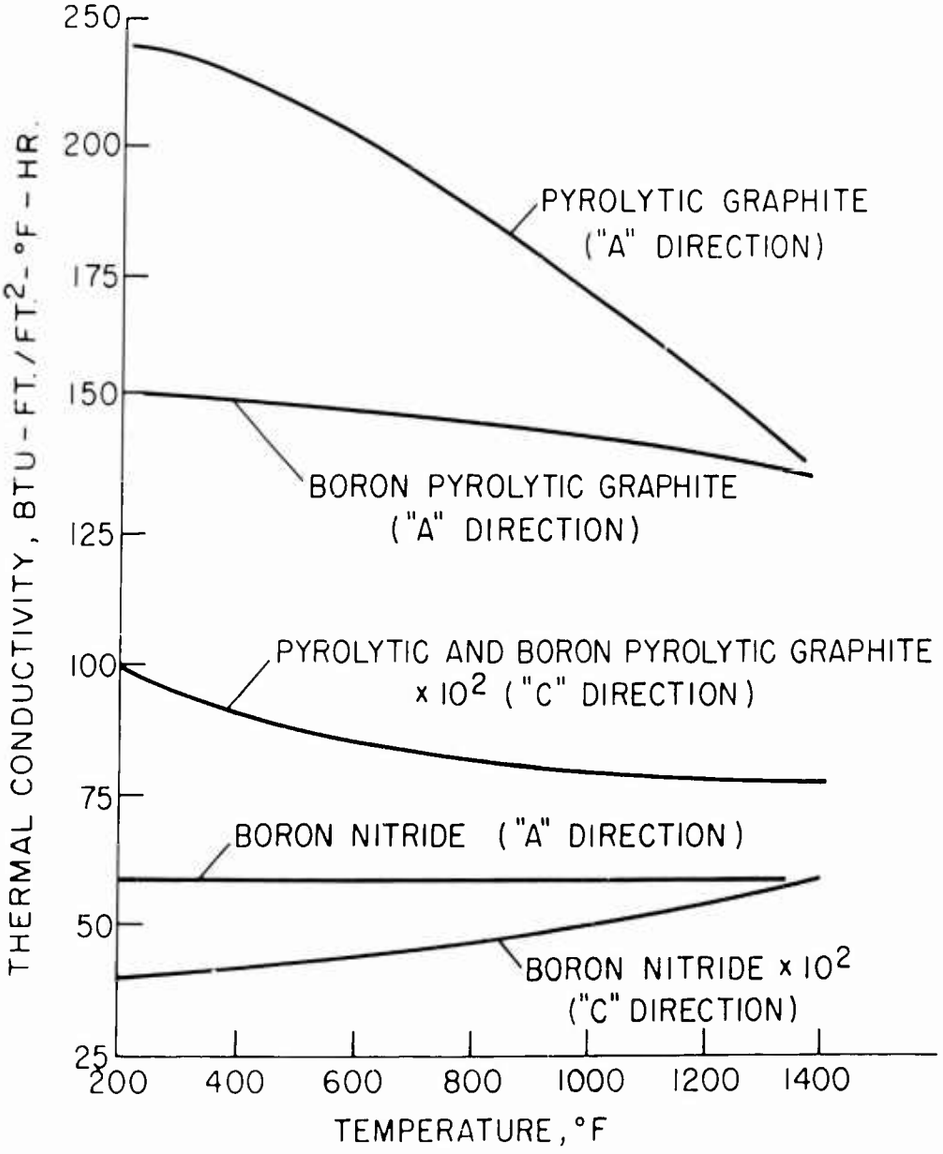

Fig. 12. Thermal Conductivity of Pyrolytic Materials

specific heat of PG is shown in Fig. (13). Because the PG, BPG, and BN are not sufficiently characterized, these data should be used for comparative purposes alone.

OXIDATION REGIMES

If one makes use of the Arrhenius representation for the rate controlled oxidation regime as discussed earlier, it is easily seen that as the surface temperature rises above 2000°R, the rate of mass loss increases exponentially and soon depletes the local oxygen supply which is available in the hypersonic boundary layer. Consequently, the slowest step is no longer the specific chemical reaction at the surface, but rather the rate at which oxygen bearing species are transported to the surface by diffusion and convection.

Thus, one can distinguish several different oxidation regimes. At the lowest surface temperatures, one has the reaction rate controlled regime. But, as the surface temperature rises, transition to a diffusion controlled oxidation regime must occur, in which the mass loss is relatively independent of surface temperature. Finally, at sufficiently high surface temperatures ($T_w > 5000°R$), the rate of sublimation of chemical species such as C(g) and C_3(g) exceeds the oxidation rate and the process is then one of sublimation. For graphite, the term "sublimation" should, of course, be reserved for the regime of extremely high surface temperatures. In Fig. (14), we have shown a representation of these different regimes. Note that, eventually, at sufficiently high surface temperatures, the vapor pressure can exceed the stagnation pressure and the boundary layer approximation $\frac{\partial p}{\partial y} = 0$ is no longer valid.

An exact solution for the mass loss has recently been obtained by Scala (9), in the diffusion controlled regime. This may be expressed:

$$\frac{\dot{m}_D \sqrt{2R_B}}{P_e^{1/2} f(\Lambda)} \left[\frac{f(\Lambda)}{\sqrt{2}}\right]^{\delta} = 6.35 \times 10^{-3} \frac{lb}{ft^{3/2}\ sec\ atm^{1/2}} \qquad (11)$$

and is shown in Fig. (15). It is noted that by definition, barring mass loss by mechanical spallation, this equation for mass loss applies equally well to pyrolytic graphite, ATJ, and in fact, all grades of carbon and graphite.

The corresponding heat transfer rate to the pyrolytic graphite in the diffusion controlled oxidation regime is given by (9):

$$\frac{Q_w \sqrt{2R_B}}{P_e^{1/2} f(\Lambda)} \left[\frac{f(\Lambda)}{\sqrt{2}}\right]^{\delta} = 33.3 + 0.0333\ (H_e - h_{w_{air}})\ \frac{BTU}{ft^{3/2}\ sec\ atm^{1/2}} \qquad (12).$$

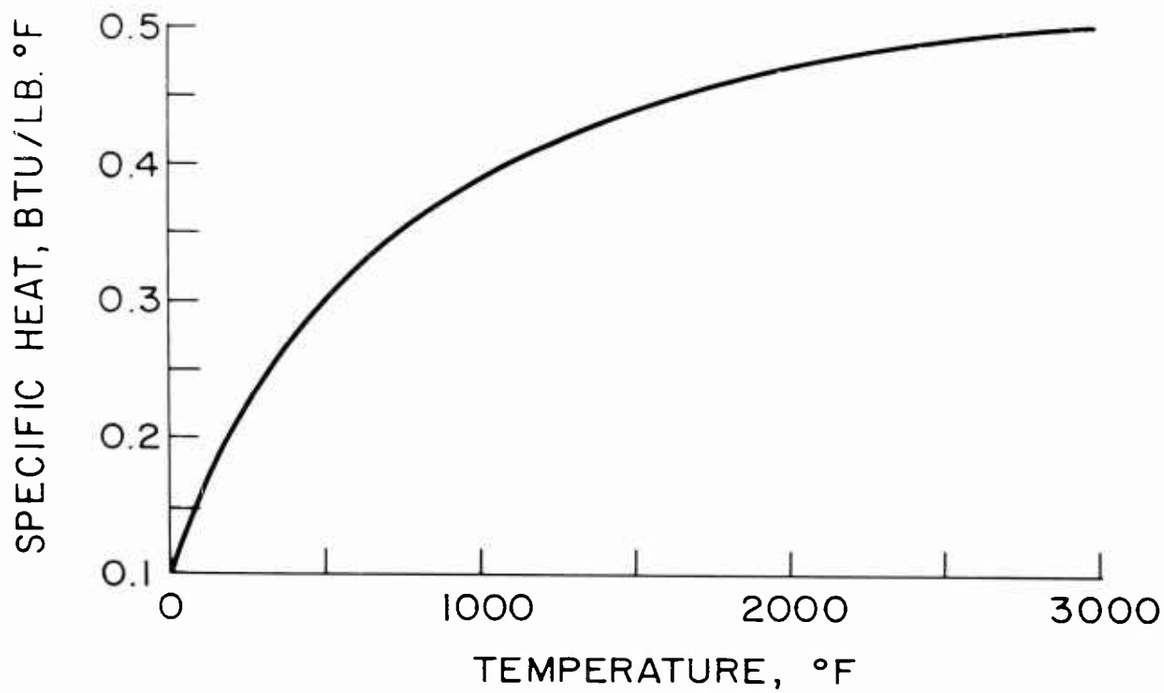

Fig. 13. Specific Heat of Pyrolytic Graphite

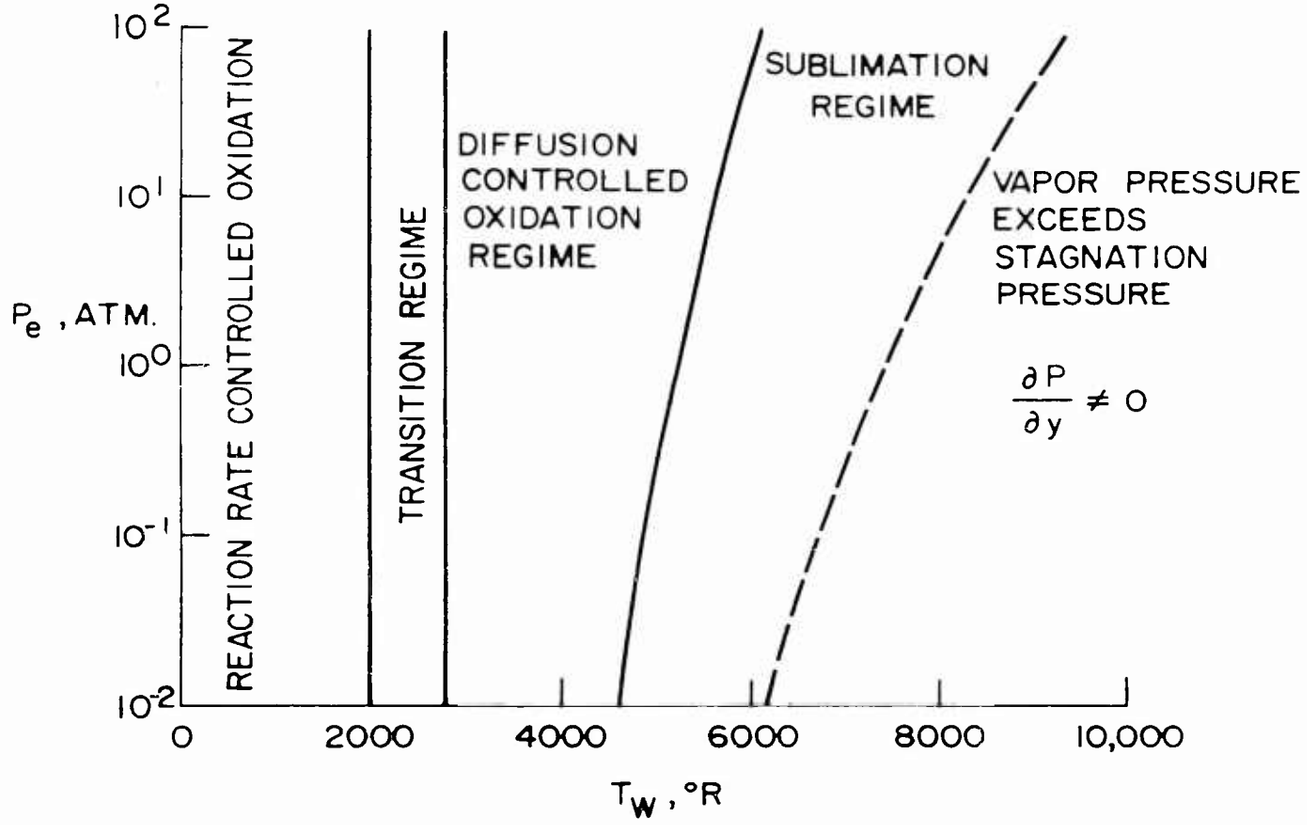

Fig. 14. Mass Transfer Regimes for Pyrolytic Graphite

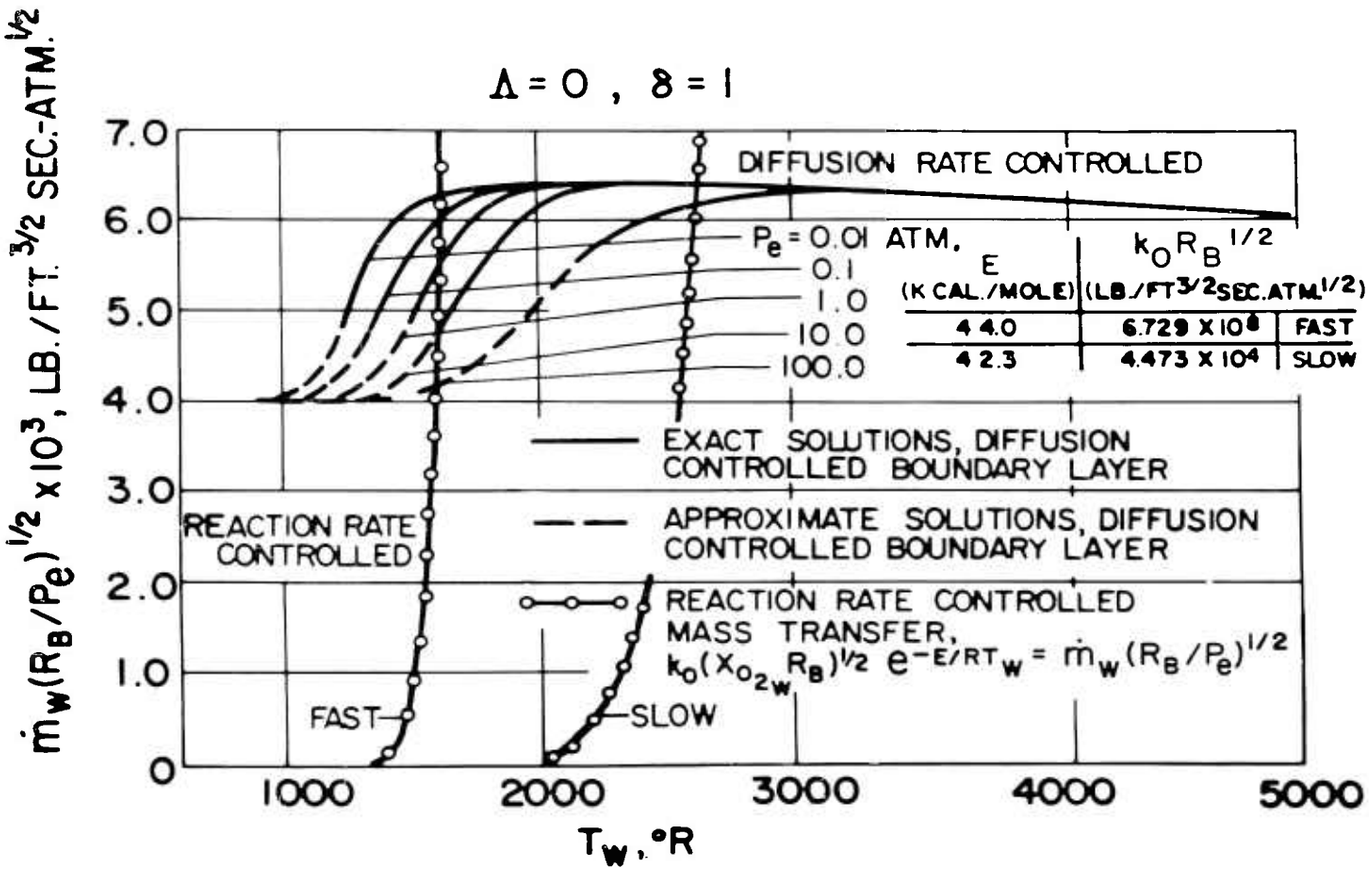

Fig. 15. Mass Transfer in Rate Controlled and Diffusion Controlled Oxidation Regimes

Here R_B is the nose radius, P_e is the local pressure over the object, Λ is the angle of yaw and $\delta = 1$ for an axi-symmetric body, while $\delta = 0$ for a two-dimensional body. A reasonable representation for $f(\Lambda)$ is given by:

$$f(\Lambda) = \cos^{3/2}\Lambda \tag{13}.$$

For the transition regime, Scala has shown that one may obtain an approximate solution for the mass transfer in the form:

$$\dot{m}_w = \frac{1}{\left[\frac{1}{(\dot{m}_R)^2} + \frac{1}{(\dot{m}_D)^2}\right]^{1/2}} \tag{14}$$

while Eq. (12) for the heat transfer rate applies to the transition and rate controlled regimes as well.

Exact solutions for the sublimation regime have just recently been obtained by Scala and Gilbert (30). In this regime, one finds that in order to account properly for the dominant aerothermochemical effects, a model is required in which one includes the relative motion of nine chemical species including O, O_2, N, N_2, CO, CO_2, CN, C(g), and C_3(g). The first four species are the four major components of dissociated iar; carbon monoxide, carbon dioxide and cyanogen are combustion products, whereas C_3 and C are the most important gaseous vaporization products. In Fig. (16), the concentrations of the predominant species present in the gas adjacent to a graphite surface, are shown as a function of surface temperature, for a pressure of one atmosphere.

When the appropriate boundary layer equations are solved, one finds, as expected, that the mass rate of sublimation increases exponentially with surface temperature. The effect of an increase in stagnation pressure is to suppress the rate of mass loss due to vaporization and the sublimation regime is shifted to higher surface temperatures. Typical results (30), are shown in Fig. (17) for stagnation pressures of 10^{-2} and 10^2 atmospheres. Here the total mass has been normalized by $\dot{m}_D$. There is a corresponding significant reduction in the heat conducted into the surface, since the mass transfer process in the sublimation regime is highly endothermic. Complete details are given in Ref. (30).

TRANSIENT THERMAL RESPONSE

The physicochemical behavior of pyrolytic graphite may be obtained by the solution of the energy equation applied to a solid whose surface is undergoing an oxidation reaction.

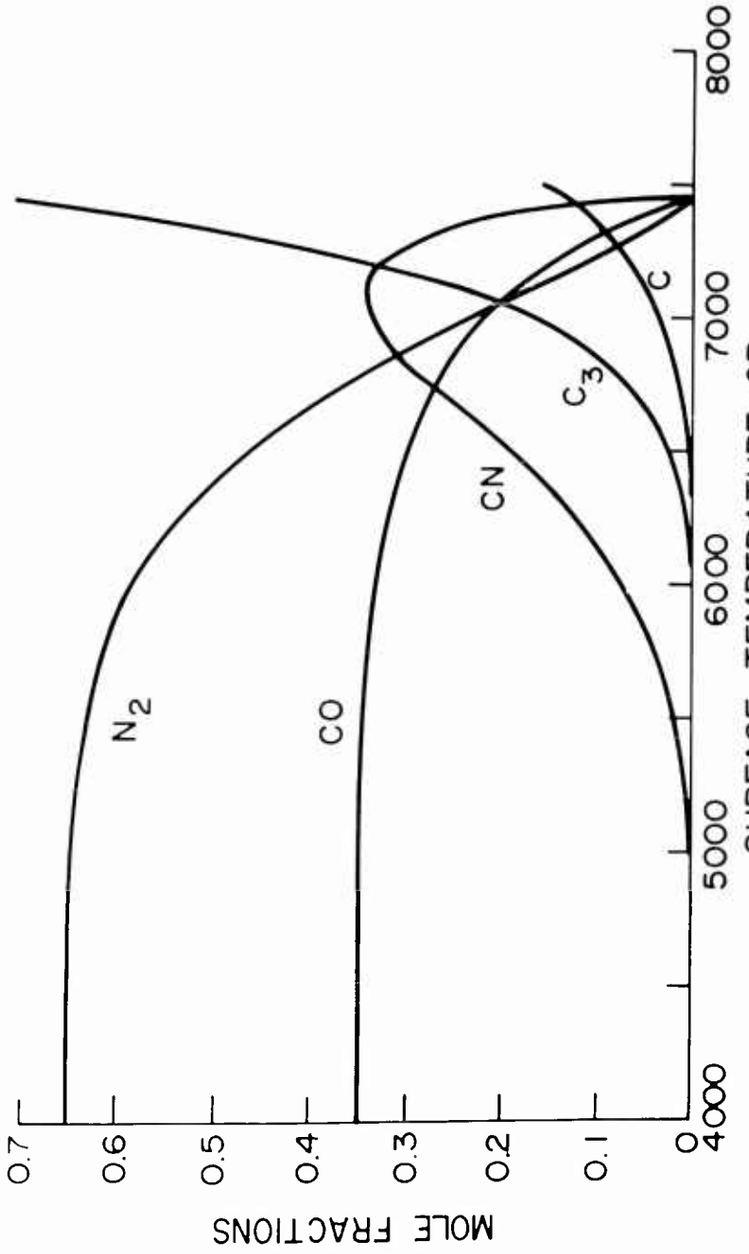

Fig. 16. Chemical Composition at a Graphite Surface, (P = 1 atm.)

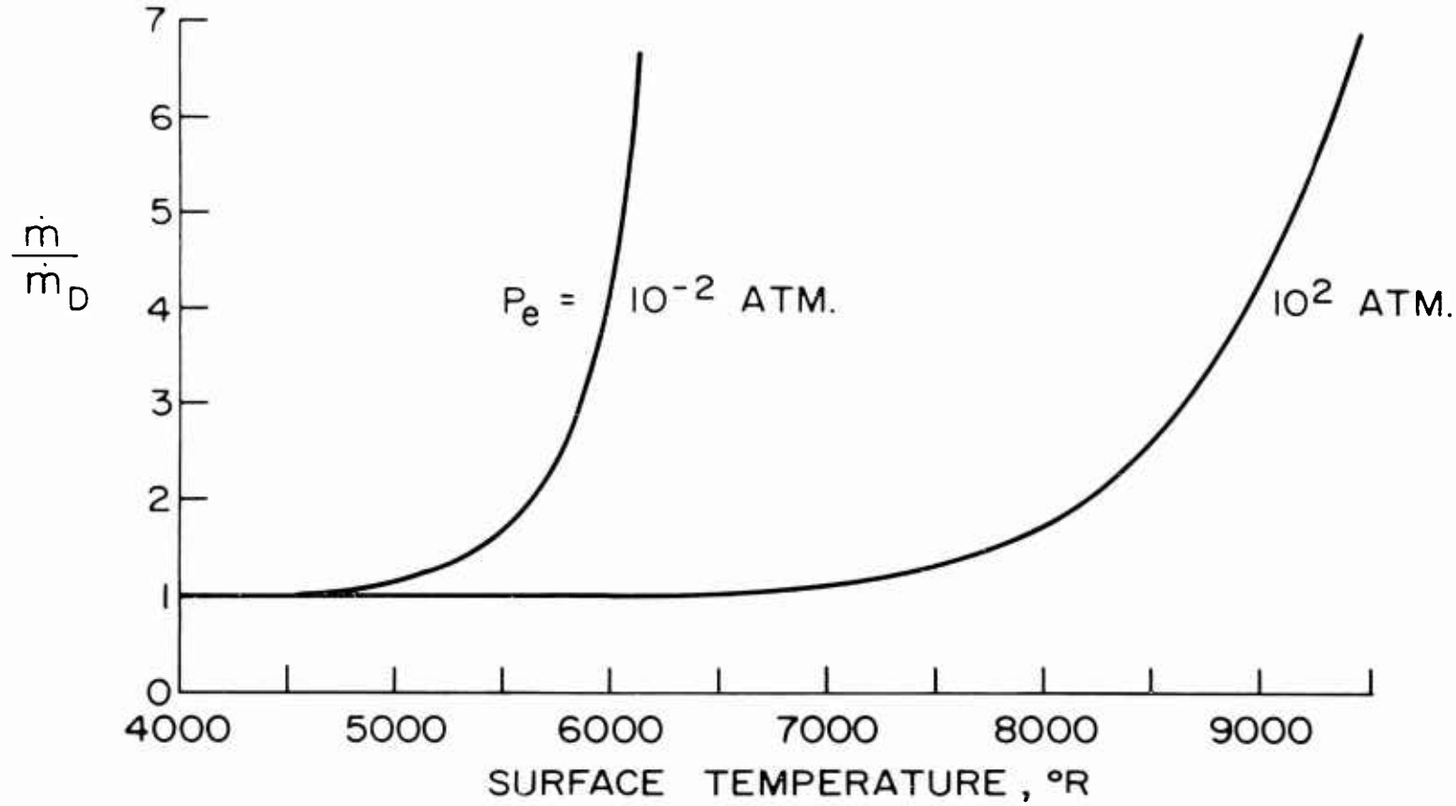

Fig. 17. Normalized Graphite Sublimation Rate

$$\rho c_p \left(\frac{\partial T}{\partial t} + \vec{v} \cdot \nabla T \right) = - \nabla \cdot \vec{Q} - \sum_i \dot{w}_i h_i \qquad (15)$$

where $\dot{w}_i$ is the chemical source term and $\vec{Q}$ is the heat flux vector. Since the chemical reactions are confined to the surface, the heat release due to chemical reaction may be consequently assigned as a boundary condition, because there are no chemical oxidation reactions occurring within the body of the solid. As a consequence, the chemical source term $\dot{w}_i$ need not appear in the fundamental equation. If one selects a coordinate system which remains stationary with respect to the moving surface rather than a coordinate system which moves with the moving surface, the convective term $\vec{v} \cdot \nabla T$ is not required and the surface oxidation appears as a boundary condition which relates the mass transfer $\dot{m}_w$ to the velocity of the moving surface $\dot{r}_w$ as follows,

$$\dot{m}_w = \rho \dot{r}_w \qquad (16).$$

In the case of an isotropic solid in which the thermal properties are not spatially dependent but are functions of temperature only, the heat flux vector $\vec{Q}$ may be written in terms of the Fourier relation

$$\vec{Q} = - K \nabla T \qquad (17).$$

This relationship then gives the familiar equation of heat conduction

$$\rho c_p \frac{\partial T}{\partial t} = \nabla \cdot (K \nabla T) \qquad (18).$$

In this equation the thermal conductivity K is a scalar temperature-dependent function.

However, when one considers a solid which is anisotropic, then the thermal conductivity is position dependent as well as temperature dependent, and consequently is a second order tensor having nine components. In the particular case of an orthotropic solid, three scalar thermal conductivity coefficients appear and the Fourier expression must be modified as follows (4):

$$-\vec{Q} = \vec{u}_1 \frac{K_1}{h_1} \frac{\partial T}{\partial u_1} + \vec{u}_2 \frac{K_2}{h_2} \frac{\partial T}{\partial u_2} + \vec{u}_3 \frac{K_3}{h_3} \frac{\partial T}{\partial u_3} \qquad (19)$$

The quantities K_1, K_2, K_3 are the three mutually perpendicular thermal conductivities; h_1, h_2, h_3 are the scale factors in the expression for the increment of arc length ds.

$$ds^2 = h_1^2 du_1^2 + h_2^2 du_2^2 + h_3^2 du_3^2 \qquad (20).$$

For specific coordinate systems, the foregoing equations may be reduced to the results given by Nolan and Scala (4). For example, the spherical coordinate system appropriate to a nose cap region may be written for the case of axially-symmetric flow:

$$\rho c_p \frac{\partial T}{\partial t} = \frac{1}{r^2} \frac{\partial}{\partial r} \left[K_r r^2 \frac{\partial T}{\partial r} \right] + \frac{1}{r^2 \sin \psi} \frac{\partial}{\partial \psi} \left[K_\psi \sin \psi \frac{\partial T}{\partial \psi} \right] \qquad (21)$$

At the stagnation point where $\psi = 0$, it is to be noted that an indeterminate form appears in the second term on the right hand side of Eq. (21). However, upon applying L'Hopital's rule to this term one finds that in the limit as ψ approaches zero, the term is finite and has the value

$$\frac{2}{r^2} \frac{\partial}{\partial \psi} \left[K_\psi \frac{\partial T}{\partial \psi} \right]$$

Hence, at the stagnation point where $\psi = 0$, Eq. (21) may be written:

$$\rho c_p \frac{\partial T}{\partial t} = \frac{1}{r^2} \frac{\partial}{\partial r} \left[K_r r^2 \frac{\partial T}{\partial r} \right] + \frac{2}{r^2} \frac{\partial}{\partial \psi} \left[K_\psi \frac{\partial T}{\partial \psi} \right] \qquad (22)$$

In cylindrical coordinates Eq. (15) becomes:

$$\rho c_p \frac{\partial T}{\partial t} = \frac{1}{r} \frac{\partial}{\partial r} \left[K_r r \frac{\partial T}{\partial r} \right] + \frac{1}{r^2} \frac{\partial}{\partial \psi} \left[K_\psi \frac{\partial T}{\partial \psi} \right] + \frac{\partial}{\partial z} \left[K_z \frac{\partial T}{\partial z} \right] \qquad (23).$$

If one assumes that the external flow over a wing or fin is two-dimensional so that cross flow does not occur along the span, then $\frac{\partial T}{\partial z}$ may be set equal to zero in Eq. (23).

We may now discuss boundary conditions appropriate to Eqs. (21) and (23). At time $t=0$, the temperature distribution within the solid may be either constant or a prescribed function of space. That is,

$$T(r, \psi, 0) = f(r, \psi) \qquad (24).$$

But because of chemical reaction, i.e., oxidation at the surface, the location of the outer surface is time-dependent, since the mass loss $\dot{m}_w$ is a function of surface position for given temperatures and environmental conditions. In the case of the hemisphere, the instantaneous surface recession rate may then be expressed by

$$\dot{r}(r, \psi, t) = \frac{\dot{m}_w}{\rho_w} (r, \psi, t) \qquad (25).$$

Since the heat flux is prescribed at the surface, Neumann type boundary conditions are to be imposed. For the hemisphere one obtains:

$$\frac{\partial T}{\partial r} \left[s(r, \psi, t) \right] = \frac{1}{K_r} \left[Q_{(s, t)} + \sigma \epsilon_g T_g^4 - \sigma \epsilon_w T_w^4 \right] \qquad (26).$$

In this equation, the symbol $s(r, \psi, t)$ denotes the instantaneous surface position of the outer boundary.

As has been shown by Gibson (31), the closed form solutions for moving boundaries, even in one dimension, (Stefan's problem), are restricted to a very few cases with Neumann boundary conditions involving a time dependent heat flux. Consequently, the foregoing equations with appropriate flight parameters have been programmed for high speed digital computer solution. Recently, the foregoing transient equations were extended at General Electric to include the case of multi-dimensional heat conduction in conical bodies with surface oxidation effects.

THERMOSTRUCTURAL RESPONSE

Solutions to general three-dimensional problems of thermoelasticity must satisfy the familiar equations of equilibrium and conditions of compatibility. Additionally, they must satisfy the prescribed boundary conditions at the surface of the body under consideration. These equations in tensor form are given in Ref. (32) and are listed here:

$$\sigma_{ij,\ j} + F_i = 0$$

$$\epsilon_{ij,\ k\ell} + \epsilon_{k\ell,\ ij} - \epsilon_{ik,\ j\ell} - \epsilon_{j\ell,\ ik} = 0 \qquad (27)$$

$$\sigma_{ij}\,\ell_i = T_i$$

where F_i, are the body force components, T_i are the surface force components, and ℓ_i are the normal direction cosines of the outer surface in the x_i coordinate directions.

These equations are based on purely mechanical and geometrical considerations and therefore would apply generally to any elastic solid, whether isotropic or anisotropic. The difference that exists between anisotropic and isotropic materials occurs in the stress-strain relations. For the most general case of an anisotropic elastic solid, the generalized Hooke's law relation contains 36 elastic constants. However, it can be shown by arguments based on thermodynamics that not all of these are independent and that there are 21 independent elastic constants for the general case of anisotropy. When thermal effects are taken into account, the Hooke's law relations contain six additional independent coefficients of thermal expansion. If the solid body under consideration exhibits structural symmetry with respect to a plane or about an axis, the number of independent elastic and thermal constants is reduced considerably.

Pyrolytically deposited materials exhibit symmetry with respect to three orthogonal planes and the c direction axis which is normal to the ab plane of deposition. Love (33) refers to a material exhibiting such symmetry as "transversely isotropic". However, others have suggested the terms "transversely anisotropic" and "monotropic" as more descriptive. It is shown in Ref. (32) that a material which exhibits symmetry with respect to three orthogonal planes is called an orthotropic material and has the following stress-strain relations:

$$
\begin{aligned}
\epsilon_a &= \frac{1}{E_a}\sigma_a - \frac{\nu_{ba}}{E_b}\sigma_b - \frac{\nu_{ca}}{E_c}\sigma_c + \alpha_a T \\
\epsilon_b &= -\frac{\nu_{ab}}{E_a}\sigma_a + \frac{1}{E_b}\sigma_b - \frac{\nu_{cb}}{E_c}\sigma_c + \alpha_b T \\
\epsilon_c &= -\frac{\nu_{ac}}{E_a}\sigma_a + \frac{\nu_{bc}}{E_b}\sigma_b + \frac{1}{E_c}\sigma_c + \alpha_c T \\
\epsilon_{ab} &= \frac{1}{G_{ab}}\sigma_{ab} \\
\epsilon_{bc} &= \frac{1}{G_{bc}}\sigma_{bc} \\
\epsilon_{ac} &= \frac{1}{G_{ac}}\sigma_{ac}
\end{aligned}
\tag{28}
$$

Taking the ab plane as the plane of deposition, Eq. (28) can be further specialized for the monotropic case by requiring elastic symmetry with respect to the c axis. Thus,

$$
\begin{aligned}
\epsilon_a &= \frac{1}{E_a}\left[\sigma_a - \nu_a\sigma_b - \nu_c\sigma_b\right] + \alpha_a T \\
\epsilon_b &= \frac{1}{E_a}\left[\sigma_b - \nu_a\sigma_a - \nu_c\sigma_c\right] + \alpha_a T \\
\epsilon_c &= \frac{1}{E_c}\sigma_c - \frac{\nu_c}{E_a}(\sigma_a + \sigma_b) + \alpha_c T \\
\epsilon_{ab} &= \frac{(1+\nu_a)}{E_a}\sigma_{ab} \\
\epsilon_{bc} &= \frac{1}{G_c}\sigma_{bc} \\
\epsilon_{ac} &= \frac{1}{G_c}\sigma_{ac}
\end{aligned}
\tag{29}
$$

where

$$\nu_a = \nu_{ba} = \nu_{ab}$$

$$\nu_c = \nu_{ac} = \nu_{bc} \tag{30}.$$

$$\nu_{cb} = \nu_{ca} = \nu_{ac}\,\frac{E_c}{E_a} = \nu_c\,\frac{E_c}{E_a}$$

It is more convenient to write the monotropic stress-strain relations in terms of properties in the plane of deposition; E, ν, and α (for convenience the subscript a is no longer used), and anisotropy ratios β, μ, κ, and λ are defined by:

$$\beta = \frac{E}{E_c}$$

$$\mu = \frac{G}{G_c} = \frac{E}{1+\nu}\,\frac{1}{G_c} \tag{31}.$$

$$\kappa = \frac{\alpha}{\alpha_c}$$

$$\lambda = \frac{\nu}{\nu_c}$$

Note that for an isotropic material the anisotropy ratios become equal to unity. Thus, the thermoelastic stress-strain equations for a monotropic material with the c axis as the axis of symmetry can be expressed in the following form:

$$\epsilon_a = \frac{1}{E}\left[\sigma_a - \nu\left(\sigma_b + \frac{1}{\lambda}\,\sigma_c\right)\right] + \alpha T$$

$$\epsilon_b = \frac{1}{E}\left[\sigma_b - \nu\left(\sigma_a + \frac{1}{\lambda}\,\sigma_c\right)\right] + \alpha T$$

$$\epsilon_c = \frac{1}{E}\left[\beta\sigma_c - \frac{\nu}{\lambda}\,(\sigma_a + \sigma_b)\right] + \frac{1}{k}\,\alpha T \tag{32}.$$

$$\epsilon_{ab} = \frac{1+\nu}{E}\,\sigma_{ab}$$

$$\epsilon_{bc} = \frac{1+\nu}{E}\,\mu\sigma_{bc}$$

$$\epsilon_{ac} = \frac{1+\nu}{E}\,\mu\sigma_{ac}$$

Many of the geometries that are of practical interest in aerospace structural design have dimensions in the c direction which are usually small compared to those in the ab plane, such as leading edge and nose can configurations. For these, the assumption of plane stress and plane strain can be made which will considerably simplify any analysis.

Consider a long hollow cylindrical shell of circular cross section subjected to a temperature distribution which is a function of radius only, see Fig. (18). The cylindrical coordinates r, θ, z, coincide, respectively, with the c, a, b coordinates of the monotropic material. Because of the radial symmetry of the geometry and temperature distribution, the assumption of plane strain for interior cross sections may be made. The corresponding equations of equilibrium, compatibility, and stress strain are:

$$r\frac{d\sigma_r}{dr} + \sigma_r = \sigma_\theta$$

$$\epsilon_r = \epsilon_\theta + r\frac{d\epsilon_\theta}{dr}$$

$$\epsilon_r = \frac{\beta - (\nu/\lambda)^2}{E}\sigma_r - \frac{\nu(1+\nu)}{\lambda E}\sigma_\theta + \left(\frac{1}{\kappa} + \frac{\nu}{\lambda}\right)\alpha T \qquad (33).$$

$$\epsilon_\theta = \frac{1-\nu^2}{E}\sigma_\theta - \frac{\nu(1+\nu)}{\lambda E}\sigma_r + (1+\nu)\alpha T$$

The above equations can be reduced to one governing equation for the radial stress:

$$\frac{d^2\sigma_r}{dr^2} + \left\{\frac{3}{r} - \frac{1}{E}\frac{dE}{dr}\right\}\frac{d\sigma_r}{dr} + \frac{1}{1-\nu}\left\{\frac{\nu\left(\frac{1+\lambda}{\lambda}\right) - 1}{E_r}\frac{dE}{dr}\right.$$

$$\left. + \frac{1}{r^2(1+\nu)}\left[(1-\beta) + \nu^2\left(\frac{1-\lambda^2}{\lambda^2}\right)\right]\right\}\sigma_r = \qquad (34)$$

$$\frac{\Omega}{r^2}\frac{T}{1+\nu}\left[\left(\frac{1-k}{\kappa}\right) + \nu\left(\frac{1-\lambda}{\lambda}\right)\right] -$$

$$\left.\frac{rT}{\alpha}\frac{d\alpha}{dr} - r\frac{dT}{dr}\right\}$$

where

$$\Omega = E\alpha/(1-\nu)$$

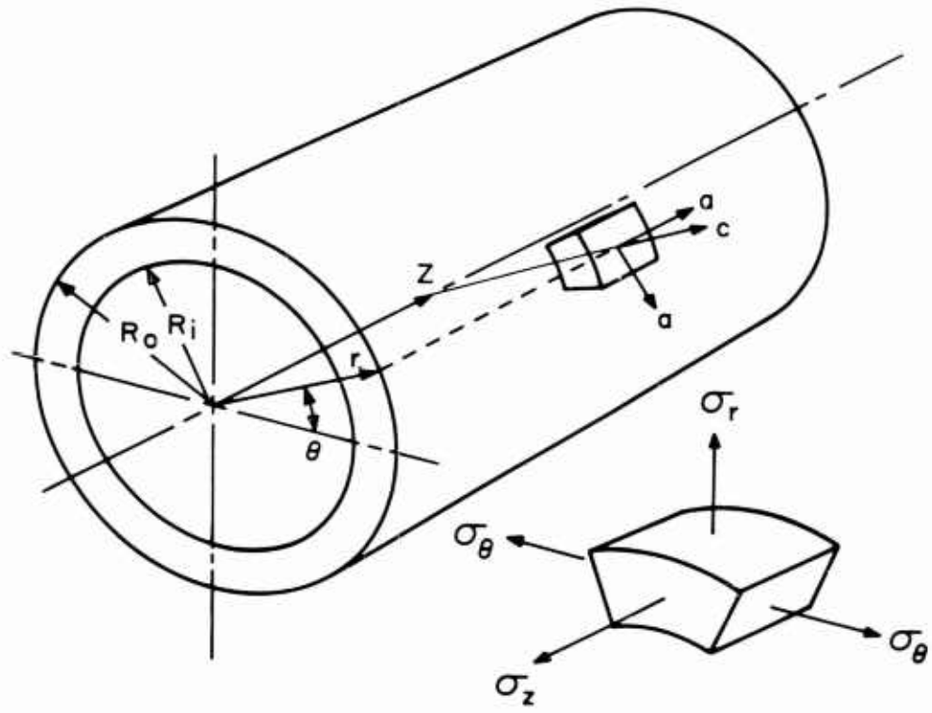

Fig. 18. Cylindrical Shell Coordinate System

The tangential stresses can be computed directly from the equation of equilibrium, Eq. (33). In certain cases it may be possible to ignore the variation of mechanical properties with temperature. For such a case, Eq. (34) reduces to a much simpler form:

$$r^2 \frac{d^2\sigma_r}{dr^2} + 3r \frac{d\sigma_r}{dr} + \Psi_c \sigma_r = \Phi_c T - \Omega_r \frac{d'T}{dr} \tag{35}$$

where

$$\Psi_c = 1 - \frac{\beta - (\nu/\lambda)^2}{1 - \nu^2}$$

$$\Phi = \left[\left(\frac{1-\kappa}{\kappa}\right) + \nu \left(\frac{1-\lambda}{\lambda}\right)\right] \frac{\Omega}{1+\nu} \tag{36}$$

For the isotropic cylinder, the anisotropy ratios β, λ, and κ are equal to one, and Eq. (34) reduces to:

$$\frac{d^2\sigma_r}{dr^2} + \left[\frac{3}{r} - \frac{1}{E}\frac{dE}{dr}\right] \frac{d\sigma_r}{dr} - \left[\left(\frac{1-2\nu}{1-\nu}\right) \frac{1}{Er} \frac{dE}{dr}\right] \sigma_r = - \frac{\Omega}{r^2} \left(\frac{rT}{\alpha}\frac{d\alpha}{dr} + r\frac{dT}{dr}\right) \tag{37}.$$

For constant mechanical and thermal properties, Eq. (37) becomes:

$$r^2 \frac{d^2\sigma_r}{dr^2} + 3r \frac{d\sigma_r}{dr} = - \frac{E\alpha}{1-\nu} r \frac{dT}{dr} \tag{38}.$$

The most significant difference between the behavior of the monotropic cylinder, Eqs. (34) and (35), and the isotropic cylinder, Eqs. (37) and (38), is associated with the fact that the monotropic equations possess a term on the right-hand side of the differential equation which is proportional to the local temperature, in addition to a term involving a variation of temperature with radius. A monotropic cylinder free from any external constraint will then develop thermal stresses while moving from one uniform temperature environment to another. This is caused by the unequal thermal expansion coefficients α and α_c which give rise to internal geometric constraints causing thermal stresses to be created. Another interesting feature of the monotropic body is that the nature of the stress state depends on the anisotropy ratios β, λ, and κ. Thus, when a hollow cylinder is subjected to a temperature gradient through the thickness such that the outer radius is at a higher temperature than the inner radius, it is usually anticipated that compressive tangential stresses will exist at the outer radius and tensile

tangential stresses at the inner radius. The corresponding radial stress distribution would then be tension throughout the thickness. This stress distribution always occurs for the isotropic cylinder. However, for the monotropic cylinder, depending on the geometry and anisotropy ratios, a complete reversal can occur -- that is, the radial stress distribution may be compressive throughout the thickness and the tangential stresses at the inner and outer surfaces are compressive and tensile, respectively. This is an extremely important factor in design, since the compressive c direction strength of pyrolytic graphite materials is much greater than the tensile c direction values.

THERMAL STRESSES IN A SPHERICAL SHELL

Consider now a spherical shell of inner radius R_i and R_o subjected to a temperature distribution which is a function of radius only, Fig. (19). The deposition geometry is such that the middle plane of the shell coincides with the plane of deposition. Thus, the governing equations of equilibrium, compatibility, and stress strain are:

$$r \frac{d\sigma_r}{dr} + 2\sigma_r = 2\sigma_\theta$$

$$\epsilon_r = \epsilon_\theta + r \frac{d\epsilon_\theta}{dr}$$

$$\epsilon_r = \frac{1}{E}\left[\beta\sigma_r - 2\frac{\nu}{\lambda}\sigma_\theta\right] + \frac{1}{\kappa}\alpha T \qquad (39).$$

$$\epsilon_\theta = \frac{1}{E}\left[(1-\nu)\sigma_\theta - \frac{\nu}{\lambda}\sigma_r\right] + \alpha T$$

The above equations can be combined in the same manner as that used for the cylinder, resulting in the following differential equation for the radial stresses in a monotropic sphere:

$$\frac{d^2\sigma_r}{dr^2} + \left[\frac{4}{r} - \frac{1}{E}\frac{dE}{dr}\right]\frac{d\sigma_r}{dr} + \frac{2}{1-\nu}\left\{\frac{\nu\left(\frac{1+\lambda}{\lambda}\right) - 1}{Er}\frac{dE}{dr} + \frac{1}{r^2}\left[(1-\beta) + \nu\left(\frac{1-\lambda}{\lambda}\right)\right]\right\} \sigma_r = \frac{2\Omega}{r^2}\left\{T\left(\frac{1-\kappa}{\kappa}\right) - \frac{rT}{\alpha}\frac{d\alpha}{dr} - r\frac{dT}{dr}\right\} \qquad (40).$$

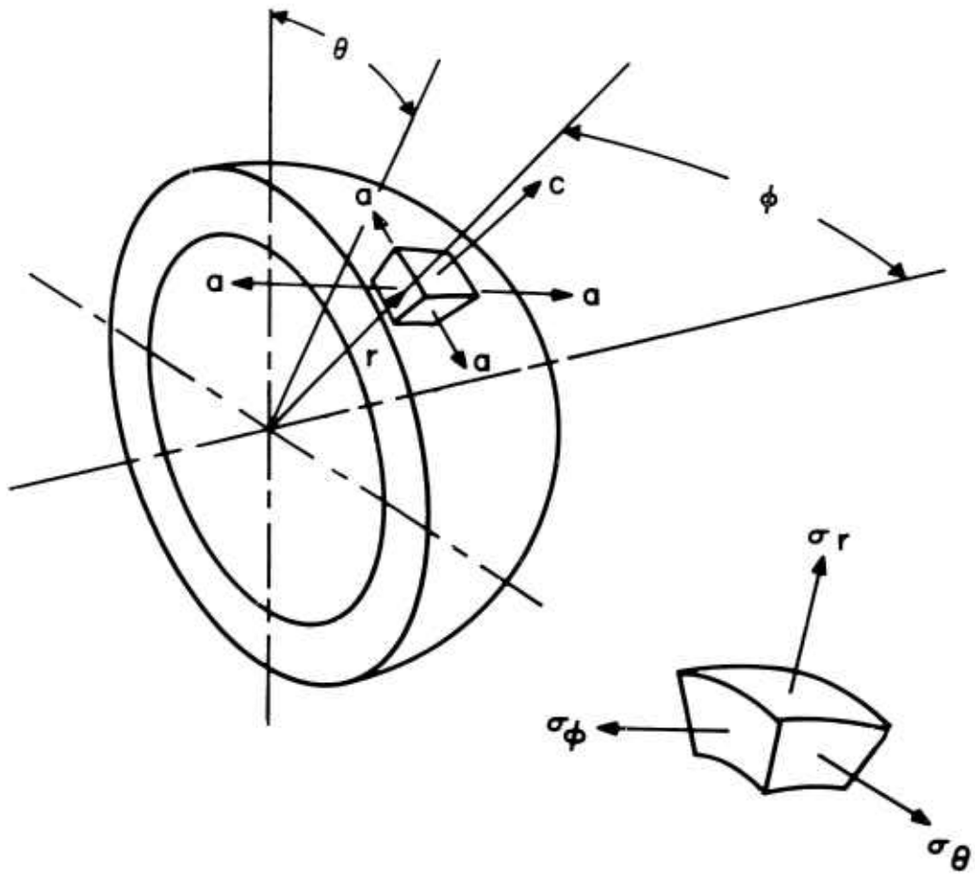

Fig. 19. Spherical Shell Geometry

The tangential stresses can be computed directly from Eq. (39). If the mechanical properties are held constant with temperature, Eq. (40) reduces to:

$$r^2 \frac{d^2\sigma_r}{dr^2} + 4r \frac{d\sigma_r}{dr} + \Psi_s \sigma_r = \Phi T - 2\Omega r \frac{dT}{dr} \tag{41}$$

where

$$\Psi_s = 2 \left[1 - \frac{\beta - \frac{\nu}{\lambda}}{1 - \nu} \right] \tag{42}$$

$$\Phi_s = 2 \left(\frac{1 - \kappa}{\kappa} \right) \Omega \tag{43}.$$

The isotropic forms of Eqs. (40) and (41) are

$$\frac{d^2\sigma_r}{dr^2} + \left[\frac{4}{r} - \frac{1}{E} \frac{dE}{dr} \right] - \frac{2(1 - 2\nu)}{1 - \nu} \frac{1}{Er} \frac{dE}{dr} \sigma_r = - \frac{2\Omega}{r^2} \left[\frac{rT}{\alpha} \frac{d\alpha}{dr} + r \frac{dT}{dr} \right] \tag{44}$$

and

$$r^2 \frac{d^2\sigma_r}{dr^2} + 4r \frac{d\sigma_r}{dr} = - 2\Omega r \frac{dT}{dr} \tag{45}.$$

Inspection of Eqs. (40) to (45) indicates that the comments made earlier regarding the differences in behavior between the monotropic and isotropic cylinder apply equally well to the spherical shell.

RESIDUAL STRESS

Among the many unusual characteristics which arise from the monotropic nature of pyrolytically deposited materials is the extreme importance of residual stresses in producing sound "as deposited" hardware. It is apparent that the thermal anisotropy, which is desirable from a thermal protection viewpoint, can result in residual stresses which can be detrimental to the structural integrity of the component. That is, in addition to the primary concern of affecting structural integrity during extreme re-entry environmental loadings, these residual stresses present a fundamental problem insofar as their effect upon the production yield of flight hardware, including producing "as deposited" shapes, machining to flight thickness, and machining of holes. The effects

which contribute to the residual stress state of structural elements fabricated from pyrolytic materials are listed below.

1. General Anisotropy
2. Growth
3. Thickness Temperature Drop
4. Nodules
5. Radial Anisotropy
6. Non-Uniform Axial Temperature
7. Asymmetric Effects
8. Geometric Discontinuities

General anisotropy is associated with those residual stresses which arise upon cooling to room temperature from deposition temperature (about 4000°F). This effect is one of the major causes of residual stresses in pyrolytic materials and is due to the monotropic character of the material. On thin-walled pyrolytic graphite nose caps, the circumferential and meridional stresses are compressive on the outside and tensile on the inside. Radial stresses are tensile and reach their maximum value in the interior of the thickness. On cylindrical and conical flare sections, the circumferential stresses are compressive on the outside surface and tensile on the inside. Meridional stresses are smaller in magnitude and of opposite sign. The radial stresses are of the same sense as those in the nose cap region. Since the allowable tensile strengths of pyrolytic graphite are low in the c direction, any effect which tends to delaminate the material, such as general anisotropy, must be carefully studied.

The biaxial stresses which result from the anisotropic expansion coefficient and the high deposition temperature are theoretically calculable for geometrically homogeneous shapes, such as cylinders and spheres, from the equations presented earlier. For a given geometry, the general anisotropy stresses are a function of the thickness to radius ratio. For a sphere, the maximum tensile and compressive tangential stresses increase linearly with t/R, Fig. (20). The maximum radial stress in the sphere increases approximately as the square of t/R, Fig. (21).

The major contribution to residual stress, other than pure anisotropy, is the stress induced by variable lattice transformation of "growth" during the deposition process. In order to explain these stresses, it is first necessary to discuss lattice transformation and the characteristics of the deposition process. Lattice transformation is a phenomenon of dimensional change of the lattice due to soaking at high temperature. The dimensional change in the macroscopic piece is therefore an increase in length and circumference and a decrease in thickness. For any given temperature, there is a definite maximum change or transformation. As the temperature increases, the amount of change increases. The kinetics of transformation are first order with respect to temperature, so that, as the temperature increases, the rate of transformation increases. A plot of dimensional change versus time will show an exponential rise to an asymptotic value for any given temperature.

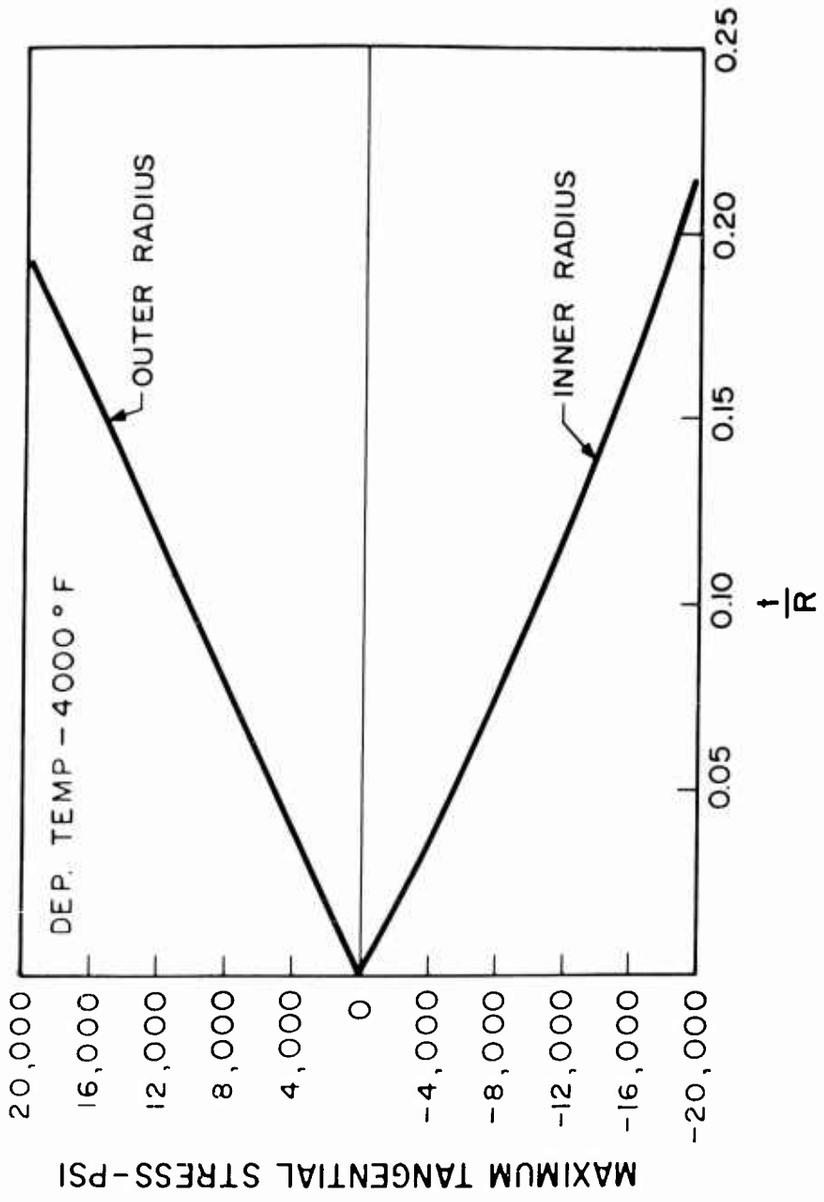

Fig. 20. Tangential Residual Stresses due to General Anisotropy

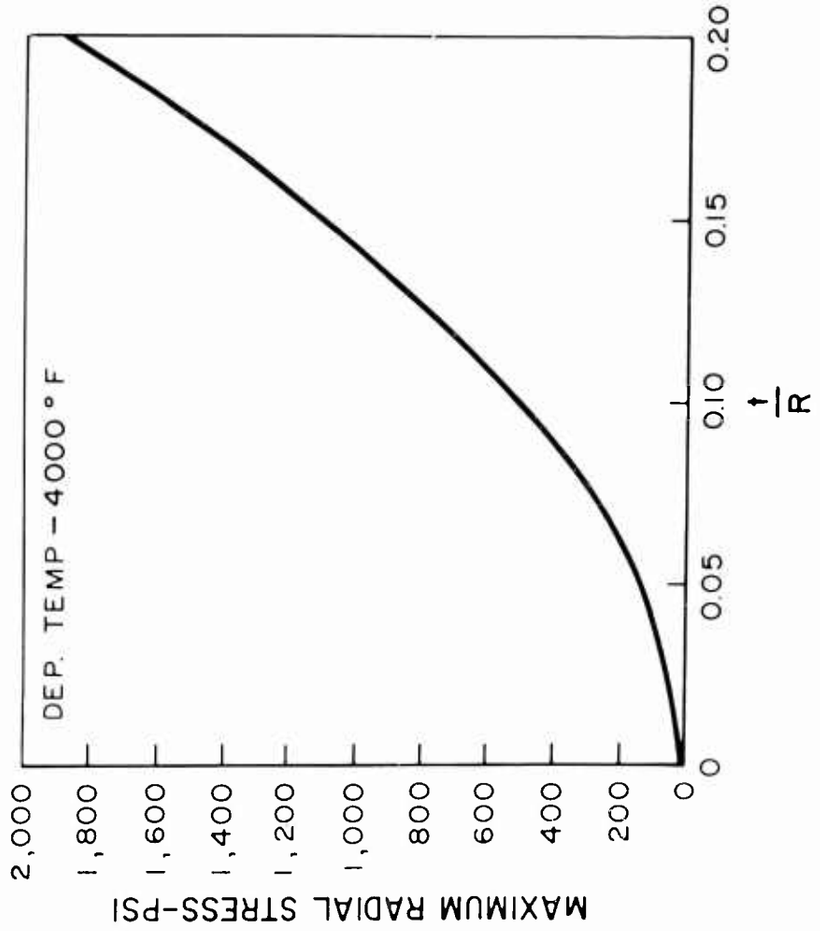

Fig. 21. Radial Residual Stresses due to General Anisotropy

The time of deposition for typical pyrolytic graphite hardware can vary from as low as 10 to 12 hr. to as high as 130 hr. Considering any given run, the initial layer is deposited within several micro-seconds; the succeeding layers are built up continuously at an essentially constant rate until the last layer is deposited and then the furnace is turned off. Immediate cooling takes place. The first layers are exposed to the deposition temperature for the total time, and each succeeding layer is exposed for less time until the final layer which is essentially unexposed. The time temperature history of each layer is, therefore, different and the different "growths" set up biaxial distributions which are opposite in sign to the general anisotropy residual stresses, which is an important consideration in designing sound "as deposited" hardware.

A further factor to consider here is the role of the mandrel in the "growth" stress picture. The mandrel, being commercial graphite, does not undergo dimensional change at the deposition temperature and therefore acts as a constraining fixture. The growth causes the mandrel and any previously deposited material to be expanded. When the deposition layer is sufficiently thick, sufficient tension is built up in the mandrel to fracture it. The mandrel falls off and the subsequent deposition takes place on the previously deposited material. As deposition continues, the first deposited layers are pushed farther and farther into tension by the outer layers. The final stress distribution, as a result of growth, is a residual tensile stress on the mandrel side. The magnitude of the compressive stress at the last deposited side depends on the deposition rate in addition to being a characteristic of the material, and is of the order of 10,000 psi.

Because of the complexity of the growth mechanisms, these residual stresses cannot be computed as simply as those arising from general anisotropy. The most convenient procedure is to obtain a growth stress formulation empirically. This procedure is dependent, however, upon the complete cognizance of all factors affecting growth stresses. Levy (34) has proposed a growth stress theory which assumes a very rapid rate of growth that sets up equivalent pressures and hence stresses as a result of the inherent restraints agains this growth. In order to obtain a numerical solution using this formulation, it is necessary to know the ultimate strength of the mandrel material at the temperature at which it breaks, the mandrel thickness, and the stress in the plane of a layer due to growth without changes in dimensions, i.e., fully constrained growth stress -- in addition to the geometry of the component. Further work in this area is currently under study at the General Electric Re-Entry Systems Department.

Since a vapor-deposited material such as pyrolytic graphite has good insulation characteristics in the c direction, each successive layer is deposited at a slightly lower temperature when a constant externally applied heat source is used. Accordingly, after the entire thickness has been deposited, for computational purposes, the shell can be construed as having a temperature drop across the thickness. The magnitude of this temperature drop would be proportional to the thickness deposited. However, the magnitude of this drop for the thicknesses of structures under consideration is not large, and its effect upon the residual stress picture is not a major one. Analytical techniques are available and can be easily used to compute these effects, which arise

as the shell cools down from this temperature distribution to an isothermal room temperature condition.

Nodules (abnormal growths in pyrolytic graphite that disrupt the continuity of the parallel deposit planes) were a problem during the early stages of development. They are a localized source of residual stress, as well as a point of weakness, in many cases caused by the presence of a soot particle in the flow. The analytical treatment by Levy (34), verified by experiment, showed that these stresses -- although serious for comparatively large nodules -- become secondary as the inclusion size diminishes. As the causes of their formation became known, methods were introduced in the deposition process to minimize (and, in some cases, virtually eliminate) them from the finished product. This was accomplished by the use of a better-grade graphite for mandrels and other parts, control of mandrel surface roughness, and thorough removal of surface dust from all parts.

It has also been determined experimentally that the material properties sometimes vary through the thickness of the deposit. Thus, strictly speaking, the material is transversely nonhomogeneous. The stresses that result from this source upon cooling to room temperature are comparatively small, the principal effect being a small change in the radial stress. In addition, since the gas injector is a heat sink, and since the radiative heat loss will vary inversely as the distance to the heat sink, a nonuniform axial deposition temperature exists. Again, the magnitude of this temperature variation is not large and has a small effect upon the axial residual stresses. Another source of residual stress is associated with asymmetric effects such as circumferential variations of thickness, temperature of deposition, and material properties. Because of the extremely random nature of these variations, the residual stresses arising from sources cannot be determined analytically with any accuracy. However, by proper process control during deposition these variations can be minimized and have been reduced in importance.

Deposition of pyrolytic materials on mandrels in the form of shells of revolution with finite lengths can complicate the residual stress pattern due to discontinuities associated with sudden changes in shell thickness, juncture of two shells of revolution, and a free edge at the end of a shell. While the structural effects associated with these discontinuities as well as those caused by thermal gradients tend to be absorbed via an essentially plane strain-stress action in the plane of deposition one cannot utilize the conventional theory of shells. Additional important effects caused by the anisotropy of the thermal expansion coefficients, and the low shear rigidity between layers must be taken into account. Use of the classical isotropic shell equations can result in serious errors for may cases of practical interest. The work at GE MSD associated with the development of a monotropic shell theory will be discussed later.

General anisotropy, growth, and geometric discontinuities are the major causes of residual stresses in "as depositied" hardware. These effects were not well understood during the early stages of pyrolytic material development, and as cracks and

delaminations began to occur in production material a considerable effort was spent on the study of the problem. Consequently, manufacturing limits associated with minimum curvature, size, and thickness were established and a series of nondestructive tests to evaluate the soundness of the material were developed. These nondestructive tests include dyecheck, videogauging, imagescope, and other ultrasonic and x-ray methods. The state of the art has developed to the point where today's manufacturers can deliver materials of thicknesses considered impossible several years ago.

In order to further increase the limiting thickness radius ratios for pyrolytic material components, studies have been conducted at GE-RSD to investigate the interaction between growth and general anisotropy stresses. This would apply to those portions which are beyond the effects of free edges or similar discontinuities, such as the stagnation region of nose caps and leading edges. Since growth stresses are opposite in sign to the "cool down" stresses, calculations were made to define the mandrel technology necessary to develop compressive radial growth stresses of sufficient magnitude to overcome the tensile radial general anisotropy stresses and result in a net radial compressive stress state. This would ensure a residual stress state that would be free of any tendency for the material to delaminate. The calculations indicate that it is indeed possible, for certain configurations of practical interest, to specify a mandrel geometry that will ensure net compressive radial stresses, tangential stresses within the "a" direction allowables of the material, and an overall residual stress state which is opposite to the environmental stress state. Work is currently under way to verify experimentally the theoretical calculations. This interaction between growth and general anisotropy is shown in Figs. (22) and (23) for a 6 in. boron pyrolytic graphite sphere of 0.3 in. thick. The discontinuity in the curves is due to the fracturing of the mandrel which occurs when the deposit is 0.05 in. thick. The growth stresses result in a 50 per cent reduction in the peak radial tensile stress.

DESIGN ANALYSIS TECHNIQUES

In order to properly design practical structural components fabricated out of pyrolytic materials, it is necessary to have available design analysis techniques which reliably predict the residual and environmental stress conditions in the component. Limiting the discussion to shell structures, the governing factors are then the spatial variation of the temperature distribution and the geometry of the component. Assuming that these can be expressed in some mathematical form, then it is indeed possible to cast the thermal stress problem for monotropic structures in a mathematical form that represents an exact three-dimensional approach to the problem. The major problem is in the solution of the differential equations which will yield the stresses and displacements of the structure. Even with the use of modern computer facilities, stress analysts have been unable to obtain versatile and useful design analysis techniques for isotropic shell structures by a frontal attack on the exact three-dimensional equations of isotropic elasticity. Consequently, it has been necessary to develop a theory for shells in which certain simplifications have been made in order to make the mathematical difficulties less severe. The validity of these simplifications for thin shells have been so sufficiently verified by test that stress analysts today use the

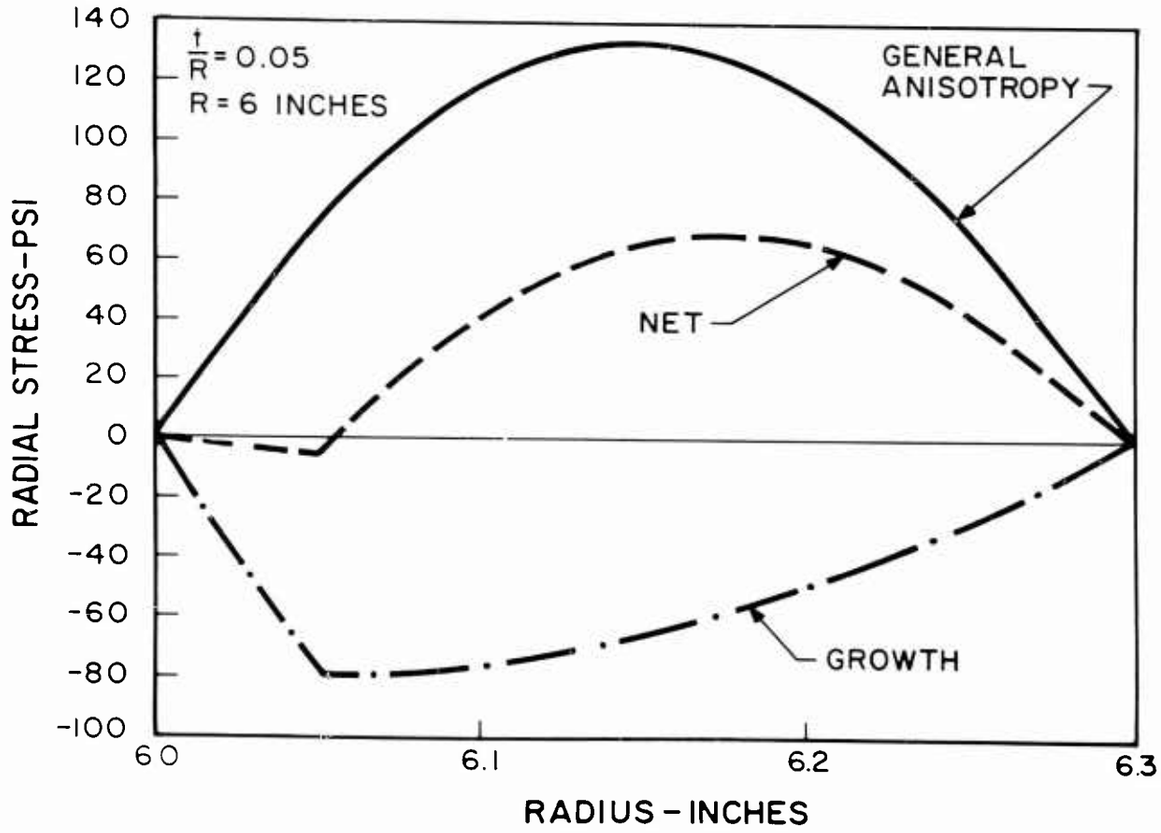

Fig. 22. Net Radial Residual Stresses in a Spherical Shell

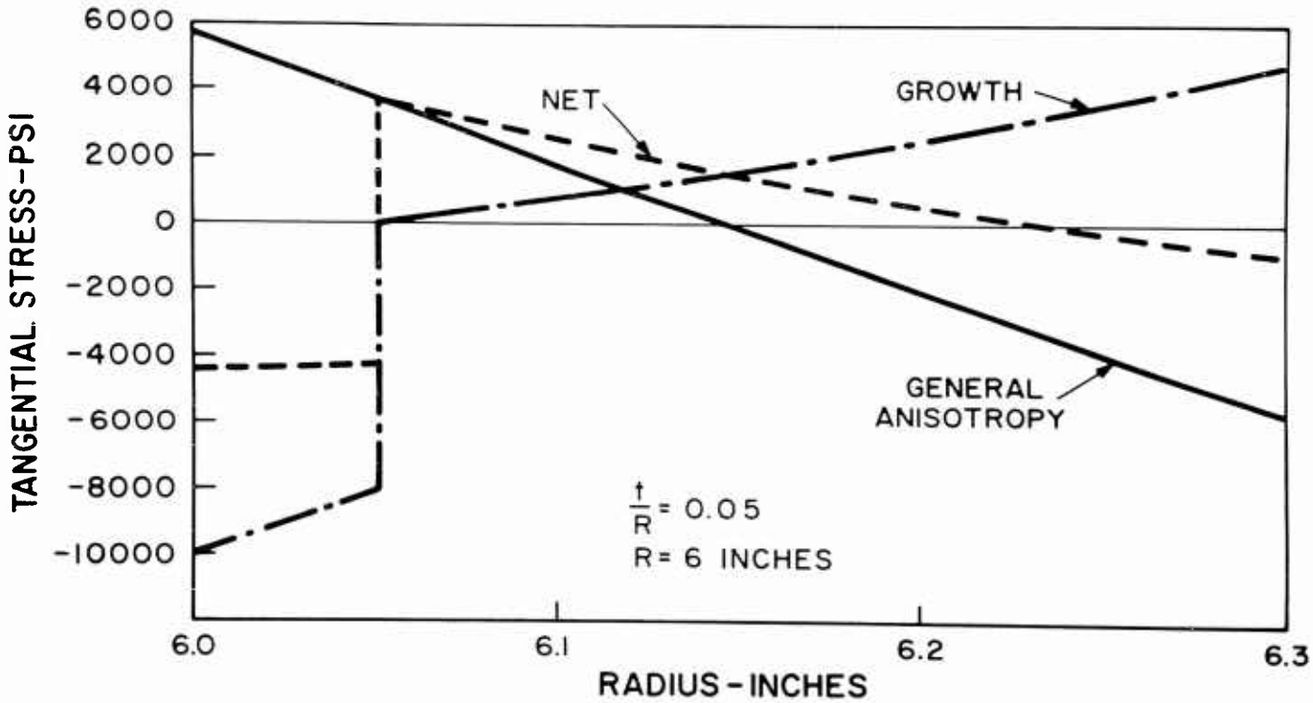

Fig. 23. Net Tangential Residual Stresses in a Spherical Shell

engineering theory for isotropic shell structures without hesitation.

The exact three-dimensional problem for monotropic shell structures presents as much, if not more, of a problem than the isotropic problem. Only in certain special limited cases as discussed previously can one obtain exact solutions. Thus, it is necessary to develop an engineering theory for monotropic shells that will enable the stress analyst to compute the thermal and environmental stresses in practical structures.

A theory for monotropic shells is under development at GE-RSD and the initial results are very encouraging. McDonough (35) has developed a shell theory for monotropic shells of revolution which takes into account the unusual thermostructural characteristics of monotropic materials. The theory was initially developed for a spherical shell and then extended to a general shell of revolution. The complete three-dimensional equations of elasticity were modified using appropriate shell approximations and the governing shell equations were obtained by direct integration. A comparison was made between the predictions of the shell theory and the complete three-dimensional solution for a symmetrically heated sphere, Figs. (24) and (25). The agreement is very good. The shell technique is currently being programmed for digital computation, for the case of the general shell of revolution.

FUTURE RESEARCH AND DEVELOPMENT

The attractiveness of pyrolytic graphite from a thermal and structural viewpoint for certain hypersonic vehicles has been established, see Refs. (3) to (6). One must not imply, however, that the ultimate has been reached for this type of material; for example, evidence has already been obtained (6), (23), that alloying the pyrolytic graphite with a small amount of boron increases both the reaction rate controlled resistance to oxidation and the tensile strength at high temperature. The possibility of producing other combinations of pyrolytic graphite and refractory substances such as hafnium, tantalum, etc. has already been investigated (29) at the General Electric Company, Missile and Space Division, as well as by others. Each combination of elements yields certain advantages not present in the others. For each of these newer materials, it will be necessary to determine the aerothermochemical performance in a hypersonic environment.

The advantages of varying the degree of anisotropy in pyrolytic graphite to minimize radial stresses during hypersonic flight have been discussed before (5) in a theoretical way. One would anticipate that the ability to produce this type of hardware would be well worth the effort invested and would open up possibilities for missions not heretofore considered.

An additional area of further development lies in the technique of high temperature bonding pyrolytic graphite to other structural members or itself. Work at GE MSD has produced useful bonding materials and techniques which have been successfully tested at temperatures ranging up to 2500°F. Since pyrolytic graphite has a thermal capability in excess of this temperature, one may conclude that effort in the art of bonding

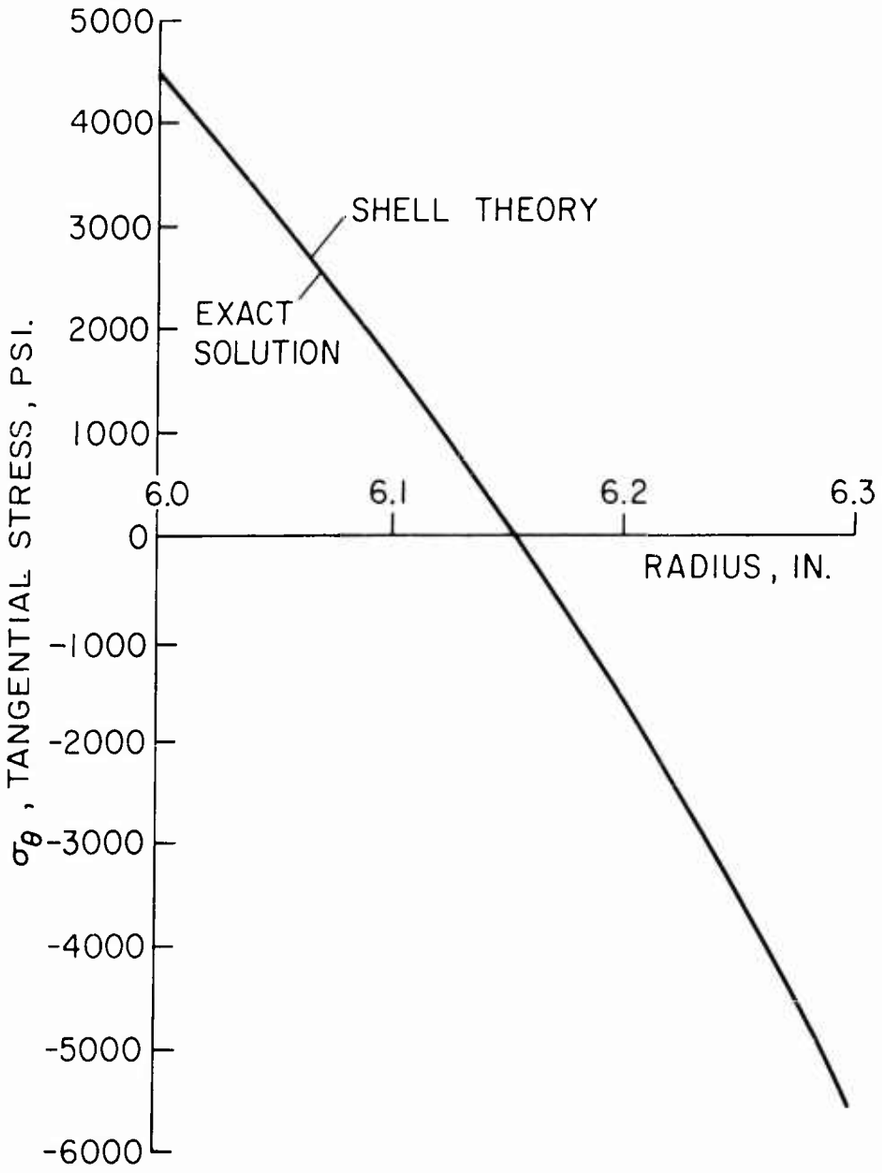

Fig. 24. Comparison of Tangential Stress Distributions

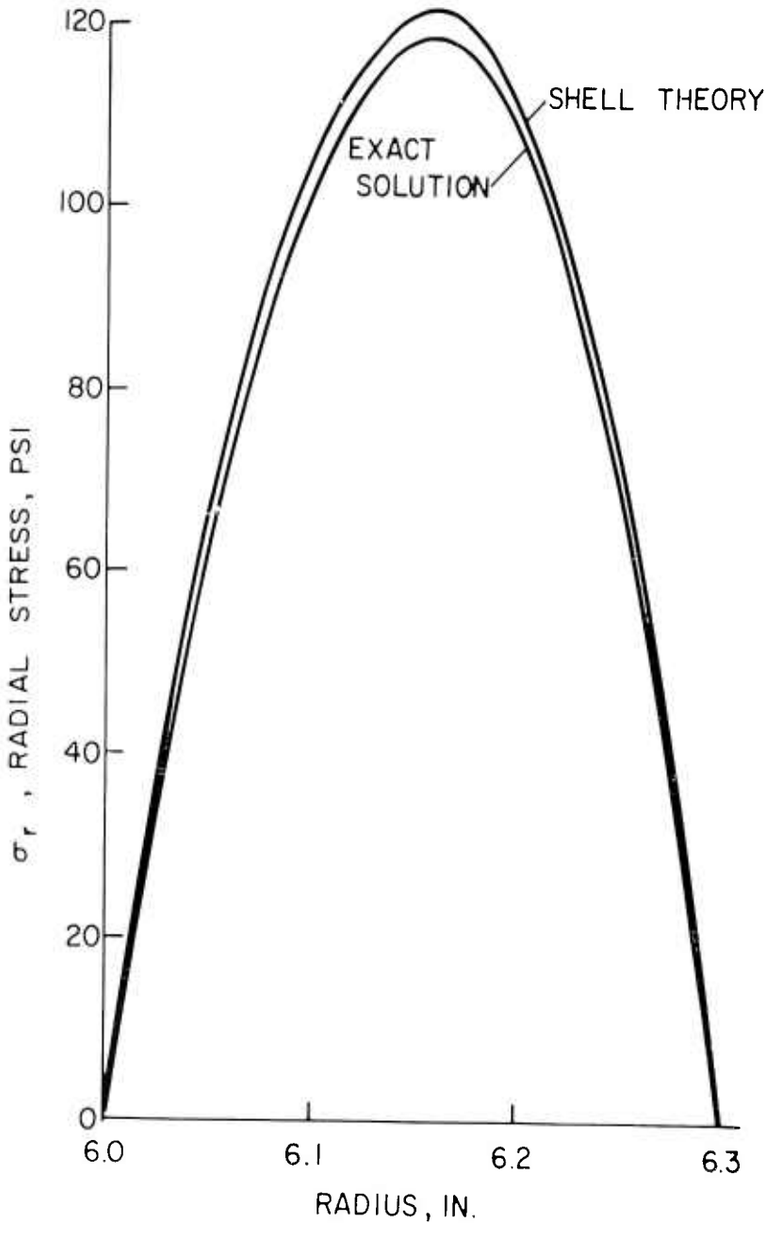

Fig. 25. Comparison of Radial Stress Distributions

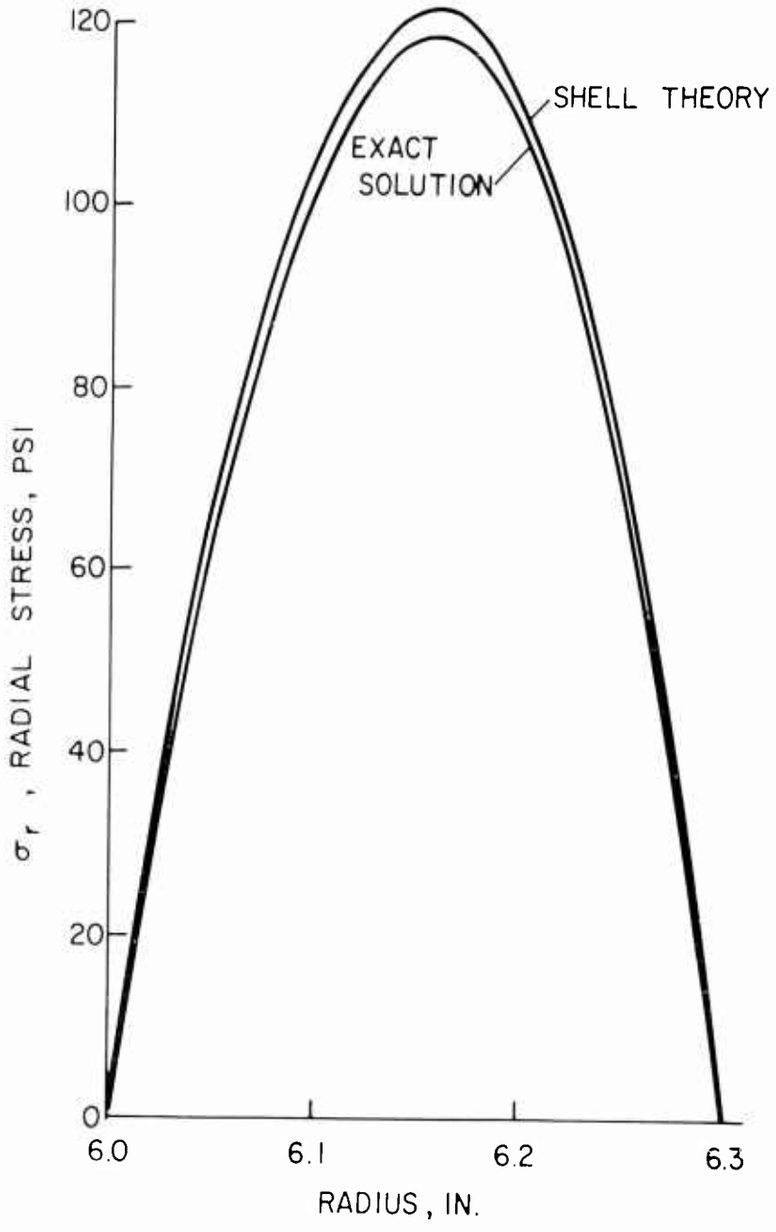

Fig. 25. Comparison of Radial Stress Distributions

has progressed substantially over that which existed only two years ago. Present indications, based on very recent effort at GE MSD (23), are that bonds for much higher temperatures can be successfully produced and applied to pyrolytic graphite. One should also comment in passing, that it may well be the case in actual practice that the bond line temperature might not exceed say 1000°F. For many hypersonic missions, sufficient time may not elapse to raise the bond line temperature any significant amount at all. This is a consequence of the low "c" direction thermal conductivity and high oxidation resistance of pyrolytic materials, (4).

Future effort in the area of material property investigations should be directed toward categorizing the performance data with a sound and identifiable material structure (23). For instance, it has already been established that the coefficient of thermal expansion is substantially affected by changes in the material structure (23). This property plays a significant role in determining the stress level both during manufacture and hypersonic flight, (6). It is apparent that more attention must be paid to this problem to assure one's self that flight hardware is indeed representative of the specimens used to measure the material properties upon which the design is based.

CONCLUSIONS

During the past several years, effort in the development of pyrolytic graphite has produced a material entirely different than that produced in the early days of 1959-1960.

Knowledge regarding the manufacturing techniques, deposition parameters, mandrel design and characterization of the material structure has been significantly increased since 1961. The art has progressed to the point where intricate shapes may now be made in varying thicknesses, whereas just one year ago such a product was thought to be impossible using the vapor deposition process.

Reliable mechanical data have now been obtained at temperatures to 5000°F. These data show that the strength at high temperatures is indeed beyond any other known material. Analytical techniques not known two years ago have now been developed and confirmed to predict not only the hypersonic flight response but the stress state of the manufactured piece as well. As a consequence of these techniques, an awareness of the importance of relating a well-characterized structure to the material properties has resulted, and renewed effort is already underway to correlate this data.

Even though a complete array of high temperature data is not available, enough data now exists to enable one to design experimental flight hardware using pyrolytic graphite.

SYMBOLS

c_p specific heat at constant pressure

E	activation energy, modulus of elasticity
F	body force
G	shear modulus
h	enthalpy
h_1, h_2, h_3	scale lengths
H	stagnation enthalpy
k	specific reactivity
k_o	effective collision frequency
K	thermal conductivity
ℓ_j	direction cosines
$\dot{m}$	mass transfer rate
n	order of the reaction
P	local static pressure
Q	heat transfer rate
r	radius, radial component
$\dot{r}$	recession rate
R	gas constant
R_B	nose radius
s	instantaneous location of the moving boundary
t	time
T	temperature, surface force
u	unit vector
x	coordinate
X	mole fraction
$\vec{v}$	velocity
z	axial component
β	defined in Eq. (31)
ϵ	emissivity, strain
θ	angular component

κ	defined in Eq. (31)
λ	defined in Eq. (31)
Λ	angle of yaw
μ	defined in Eq. (31)
ν	Poisson's ratio
ρ	density
σ	stress
Φ	defined in Eq. (36)
ψ	meridional angle
Ψ	defined in Eq. (36)
Ω	defined in Eq. (34)

Subscripts

a	a-b plane
D	diffusion controlled regime
e	edge of boundary layer
g	gas cap
i	species i
ij, kℓ	tensor components
R	reaction rate controlled regime
S	sublimation regime
w	wall

REFERENCES

1. Sawyer, W. E., U. S. Patent No. 229,335, 1880.

2. Clark, T. J. and Larsen, R. J., "Final Report on Work Statement No. 87, Residual Stress Studies", General Electric Co. Report P1-WS-0232, MPD Detroit, 1961.

3. Scala, S. M. and Nolan, E. J., "Aerothermodynamic Feasibility of Graphite for Hypersonic Glide Vehicles", Re-Entry and Vehicle Design, Vol. IV, Proceedings of the Fifth Symposium on Ballistic Missile and Space Technology, Academic Press, August 1960, p. 31.

4. Nolan, E. J. and Scala, S. M., "The Aerothermodynamic Behavior of Pyrolytic Graphite During Sustained Hypersonic Flight", ARS Journal, Vol. 32, No. 1, January 1962, p. 26.

5. Scala, S. M., Nolan, E. J. and Garber, A. M., "The Aerothermoviscoelastic Response of an Orthotropic Material During Hypersonic Flight", ARS Preprint 2150-61, Space Flight Report to the Nation, October 1961.

6. Garber, A. M. and Nolan, E. J., "Thermal Stresses in Pyrolytic Graphite During Sustained Hypersonic Flight", Dynamics of Manned Lifting Planetary Entry, (Edited by Scala, Harrison and Rogers), John Wiley and Sons, 1963, p. 536.

7. Hedden, K. and Wicke, E., "About Some Influences on the Reactivity of Carbons", Proceedings of the Third Conference on Carbon, Pergamon Press, 1959, p. 249.

8. Blakeley, T. H., "The Gasification of Carbon in Carbon Dioxide and Other Gases at Temperatures Above 900°C", Proceedings of the Fourth Conference on Carbon, University of Buffalo, 1959.

9. Scala, S. M., "The Ablation of Graphite in Dissociated Air, Part I, Theory", IAS National Summer Meeting Paper No. 62-154, June 1962. Also General Electric Co. Document TIS R62SD72.

10. Horton, W. S., "Oxidation Kinetics of Pyrolytic Graphite", General Electric Co., G. E. L., Document No. 60GL218, January 1961.

11. Streznewski, J. and Turkevich, J., "The Reaction of Carbon with Oxygen Atoms", Proceedings of the Third Conference on Carbon, Pergamon Press, 1959, p. 273.

12. Brown, A. R. G., Hall, A. R. and Watt, W., "Density of Deposited Carbon", Nature, Vol. 172, 1953, p. 1145.

13. Brown, A. R. G., Watt, W., Powell, R. W., and Tye, R. P., "Thermal and Electrical Conductivities of Deposited Carbon", British Jour. Appl. Phys., Vol. 7, 1956, p. 73.

14. Brown, A. R. G. and Watt, W., Industrial Carbon and Graphite, Society of Chemical Industry, London, 1958, p. 86.

15. Brown, A. R. G., Brown, D. and Estabrook, J., "Structure and Density of Pyrolytic Carbon", J. Less Common Metals, Vol. 1, 1959, p. 94.

16. Lozier, W. W. and Manofsky, M. B., "Properties and Performance of Pyrolytic Graphite", presented at the Research Conference on the Mechanical Properties of Engineering Ceramics, No. Carolina State College, March 1960.

17. Meyer, L. and Gomer, R., Third Biennial Carbon Conference, Pergamon Press, 1959, p. 425.

18. Murphy, D. B., Plamer, H. B. and Kinney, C. R., Industrial Carbon and Graphite, Society of Chemical Industry, 1958, p. 77.

19. Conroy, J. S., Slysh, R. S., Murphy, D. B. and Kinney, C. R., Third Biennial Carbon Conference, Pergamon Press, 1959, p. 395.

20. "Final Report on Pyrolytic Graphite", Lockheed Missile and Space Co. Report 801376, June 1962.

21. "Final Report - Pyrographite Research and Development", Raytheon Company Document 5-347, August 1961.

22. Aerojet General Corp. Reports L3742-01-1 through L3742-01-11, September 1961.

23. Mehan, R. L., "Review of Mechanical and Thermal Properties of Pyrolytic Graphite", General Electric Co., Re-Entry Systems Department Report PIR-MPL 8155-197, July 1963.

24. "Symposium on Determination of Elastic Constants", ASTM Special Technical Publications No. 129, June 1952.

25. Kotlensky, W. V. and Martens, H. E., "Tensile Behaviour of Pyrolytic Boron Nitride to 2200°C", Nature, Vol. 196, 1962, p. 1090.

26. Kotlensky, W. V. and Martens, H. E., "Tensile Properties of Hot-Worked Pyrolytic Graphite", Trans. Met. Soc. AIME, Vol. 221, 1961, p. 1085.

27. Martens, H. E. and Jaffe, L. D., "Tensile Strength of Pyrolytic Graphite up to 2750°C", J. Appl. Phys., Vol. 31, 1960, p. 1122.

28. Martens, H. E. and Kotlensky, W. V., "Tensile Behaviour of Pyrolytic Graphite at 2750°C", Nature, Vol. 186, 1960, p. 960.

29. Gebhardt, J. and Berry, J., Private Communication, September 1963.

30. Scala, S. M. and Gilbert, L. M., "Aerothermochemical Behavior of Graphite at Elevated Temperatures", Sixteenth Pacific Coast Regional Meeting of the American Ceramic Society, Los Angeles, Cal., October 24, 1963.

31. Gibson, R. E., "A Linear Problem With a Moving Interface", ZAMP, Vol. 11, 1960, p. 198.

32. Sokolnikoff, I. S., Mathematical Theory of Elasticity, Second Ed., Chap. 3, McGraw Hill Book Co., Inc., 1956.

33. Love, A. E. H., A Treatise on the Mathematical Theory of Elasticity, Dover Publ., Fourth Ed., 1944.

34. Smith, W. H., "Final Report on Work Statement No. 94a Improved Task III Units", General Electric Co., Met. Prod. Dept. Rept. P1-WS-0207, 1961.

35. McDonough, T. B., "Monotropic Shell Theory", General Electric Co., Re-Entry Systems Dept. T. M. 8156-36, February 1963.

ACKNOWLEDGMENT

The authors wish to acknowledge the assistance of Mr. R. L. Mehan in the compilation of the thermal and structural property data and Mr. L. Gilbert in the compilation of the chemical property data. The numerical results were obtained by Messers. F. Bosworth and J. Massey who programmed the equations for the IBM 7094 digital computer.

This paper is based in part on work which was supported by USAF BSD AFSC under Contract No. AF 04(694)-222.

RE-ENTRY SYSTEMS DEPARTMENT
AND
SPACE SCIENCES LABORATORY
MISSILE AND SPACE DIVISION

GENERAL ELECTRIC

TECHNICAL INFORMATION SERIES

AUTHOR	SUBJECT CLASSIFICATION	NO.
A. M. Garber E. J. Nolan S. M. Scala	Pyrolytic Graphite	R63SD84
		DATE: October, 1963
TITLE: PYROLYTIC GRAPHITE - A STATUS REPORT		G. E. CLASS: 1
		GOV. CLASS: None
REPRODUCIBLE COPY FILED AT MSD LIBRARY, DOCUMENTS LIBRARY UNIT, VALLEY FORGE SPACE TECHNOLOGY CENTER, KING OF PRUSSIA, PA.		NO. PAGES: 57

SUMMARY It is the purpose of this paper to review the recent history of the development of pyrolytic graphite and its thermal, aerothermochemical, and structural properties with regard to its application to hypersonic vehicles.

Pyrolytic graphite is not really new since its discovery dates back to Thomas Edison, however, this class of refractory materials has been "rediscovered" recently because it possesses certain desirable properties at extremely high operating temperatures, including a high strength to weight ratio, low oxidation rate, and a low transverse coefficient of thermal conductivity.

Consequently, a thorough investigation of the properties of pyrolytic graphite is being carried out. In addition, theoretical models are being developed so that its aerothermochemical and aerothermostructural behavior can be predicted with confidence for arbitrary hypersonic missions. In this paper, the currently available property data, and analytical and numerical techniques are presented and discussed critically, and areas for future research and development are delineated.

By cutting out this rectangle and folding on the center line, the above information can be fitted into a standard card file.

AUTHOR A. M. Garber, E. J. Nolan, S. M. Scala

COUNTERSIGNED Dr. J. D. Stewart, Dr. J. Barber